INTERNATIONAL JOURNAL OF
ENERGY AND ENVIRONMENT

Volume 3, Issue 5, 2012 pp.809-832

Journal homepage: www.IJEE.IEEFoundation.org

Squeal analysis of ventilated disc brake using ansys

Ahmed Abdel-Naser[1], Ibrahim Ahmed[2], Essam Allam[1], Sabry Allam[2], Shawki Abouel-seoud[1]

[1] Automotive and Tractors Engineering Department., Faculty of Engineering, Helwan University, Cairo, Egypt.
[2] Automotive and Tractors Technology Department, Faculty of Industrial Education, Helwan University, Cairo, Egypt.

Abstract
It is well-known that automobile brakes can generate several kinds of noises. Among them is squeal, a noise in the 1-15 kHz range. It is commonly accepted that brake squeal is initiated by instability due to the friction forces, leading to self excited vibrations. To predict the onset of brake instability, a modal analysis of the prestressed structure can be performed on an improved dynamic finite element model of ventilated disc brake with friction coupling. An unsymmetric stiffness matrix is a result of the friction coupling between the brake pad and disc; this may lead to complex eigenfrequencies. The complex eigenvalue method (Unsymmetric solver) used to analyse mode shapes associated with the predicted natural frequency. Creating the element of Matrix27 between the ventilated disc and pad was very important in studying the squeal of the coupled ventilated disc brake. The results demonstrated that the FEM for the coupled ventilated rotor and pad showed a good interaction between the non-linear contact and the linear modal analysis. Furthermore, the unsymmetric solver showed that the modes of the coupled disc-pad contained two types of mode. The first type was normal mode, which did not contain an imaginary part while the second type was complex mode that contained real and imaginary parts. Moreover, complex eigenvalue analysis predicted always more unstable modes than the number of squeal frequencies that really occur in the brake system. The maximum squeal index was observed at mode 16 and at frequency of 4083 Hz with instability of 480 sec^{-1}. However; the tendency of instability (TOI) for the system at contact stiffness of 1 GN/m was 59 that gave the lowest instability of the system.

Keywords: Ventilated disc brake; Instability; Squeal Index; Noise Index; Eigenfrequencies.

1. Introduction

Ventilated brake discs or rotors are known as high performance brakes, and it is produced by making hollows or slots of different shapes on the disc surface and side edges. Most of the literature available on improving the operational efficiency of today's vehicle brakes in order to meet tomorrow's increasingly more difficult standards for brake dynamic performance, mode shape, contact stiffness and related squeal while maintaining acceptable derivability have been devoted to establish the relationship between vehicle brake performance criteria and squeal characteristics. Brake-induced noise and vibration are serious concerns in the automotive industry due to the annoyance to the consumers. The most common noise is squeal which is defined as noise whose frequency content is 1000 Hz or higher that leads to excessively high and irritating sound pressure levels. Resonance or high amplitudes results due to a frequency match

in linear systems, while resonance in nonlinear system may occurs at excitation frequencies that are not equal to the linear system's natural frequency. Even a harmonic excitation provided by stick–slip phenomenon may turn the system into a non-periodic or chaotic motion. Squeal has been categorized as low- and high-frequency squeals for the purpose of analysis [1, 2]. The frequency ranges for the low-frequency squeal is 1000–2600 Hz and for high frequency squeal is 2–15 kHz. The squeal is affected by the pad, rotor and brake assembly material and geometry. It does not only depend on the bulk properties of the contact surfaces but also on the surface properties. Sprag–slip effect of the shoe against the rotor has also been reported as one probable cause of squeal. Geometrically induced instability or kinematics instability also emphasizes the physical parameter`s of the system along with the coefficient of friction as a reason for squeal. System instabilities are generated due to changes in the direction of both normal and frictional forces (binary flutter theory) and are based on the dynamic characteristics of the rotor. Squeal is also attributed to the complex modes of vibration which are interpreted as travelling waves.

The squeal noise problem can be addressed through a significant number of previous studies have focused on examining brake system level design concepts, including investigations that have led to modifications made to the calliper stiffness [3, 4], mounting bracket [5, 6], and rotor geometry [7, 8]. Generally, in most cases the analyses attempted to apply the modal participation factor of each component to assess their potential effect on squeal noise occurrences. Since the modal participation factors of larger size structures, such as the rotor and calliper, are typically higher than those of the smaller components such as the pad, and minor hinges and bracket s, the effects of the lesser components have not received much attention even though they may be more economical and feasible to tackle in practice. While modal participation factors play a significant role in squeal noise, it may not be the only factor. In fact, most brake pad manufacturers currently rely on trial- and-error approaches to address brake noise concerns, which are not only time consuming and costly, but may not result in the best sets of remedies [9].

In recent years, the finite element (FE) method [10-15] has gained wide acceptance for analyzing many varieties of complex problems in structural dynamics, including some of the more intricate brake vibrations and noise problems. Although successful cases studies have been reported from time to time, no real reliable brake noise prevention tool truly exist yet. Some of recent literature reviews [16, 17] reported on the complexity and lack of understanding of the squeal problem. To our knowledge, there is no publicly reported prior analysis that tackles the pad dynamics problem to determine suitable designs with lesser tendency towards squeal production has been performed. This paper tries to find a solution for the squeal by addressing two important challenges in developing a feasible analysis tool: (i) validating the structural connections and boundary conditions critical to the true dynamic representation, and (ii) modelling the rotor– pad friction coupling mechanism essential to the self-excited excitation source.

For the second issue on rotor– pad friction model, a dynamic FE model with friction coupling that is incrementally more complex than the existing friction theories is proposed. This approach enables the effects of both structural modes and frictional excitation to be analyzed simultaneously. This modelling scheme differs from previous lumped parameter dynamic models [18-21] used mostly to examine the effects of global system parameters on self-excitation causing squeal, where the detailed pad design parameters that are of interest to the brake friction manufacturers are not typically analyzed. To ease final FE modelling, the friction coupling formulation is first developed using theoretical lumped parameter system similar to classical theories. This first order structural dynamic approximation is employed to determine the effects of system level modifications and to guide initial pad design. However, research on contact pressure distributions in a disc brake system has been carried out by a number of people. The parameter is now becoming essential to the brake research community especially to those who are predicting squeal noise using numerical methods of either the complex eigenvalue analysis or the dynamic transient analysis. There are several levels of complexity in disc brake models that have been developed in order to predict dynamic contact pressure distributions through numerical methods. Since the complex eigenvalue analysis largely depends on the contact pressure distribution, it is essential to develop a more realistic representation of the FE model [22-31].

The disc brake squeal has studied using a detailed 3-dimensional finite element (FE) model of a real disc brake [32]. It was found that there was a good agreement in squeal predictions between the FE model and experimental results. A number of structural modifications for suppressing unstable vibration were simulated. A plausible modification that results in reduced positive real parts of the eigenvalues was proposed. It was suggested that combined modification, i.e. partial connections the piston and the piston-

pad back plate and between the finger and the finger-pad back plate, a stiffer calliper and a stiffer disc can eliminate unstable frequencies below 8000Hz, which are dominant in the baseline model. Therefore, this modification is regarded as a plausible one. However, another piece of work [33] has confirmed that brake noise usually is not observed while friction is initially developing, the brake is recovering from high temperature friction film degradation or the brake temperature is rising from ambient. It was also found that the brake noise usually is associated with steady elevated brake temperatures (40-120 ºC) where the friction films on the rotor and pads are well developed and the coefficient of friction remains steady.

A theory of squeal has been presented which allows the study of the linear stability of a class of systems consisting of two subsystems coupled through a frictional contact point [34]. This feature proved to have a significant influence on stability when the contact spring stiffness takes values of the same order of magnitude or lower than that of the average structural stiffness of the system. The last and most elaborate extension consisted in allowing the coefficient of friction to vary linearly with the sliding speed. In accordance with previous results, a coefficient of friction rising with the sliding speed tends to make a system more stable, although this is not systematic. However, the analysis directed towards squeal triggering, establishment or vanishing in terms of a new index dependent on two topographic parameters has been described [35, 36]; the mean radius of asperities and the standard deviation of the height distribution of asperities of the sliding surfaces. Experimental investigation of squeal noise generated from the friction sliding of a brake pad on a rotating Plexiglas disc revealed that the pad surface at the beginning of squeal became glazed and that it abraded the disc however, the disc surface topography is not affected by the squeal.

From previous work that has been concentrated on studying the performance of vehicle brake in order to improve their characteristics. Various authors have exposed their theoretical work for the vehicle brake performance; their contributions were limited. It was found a need for more theoretical investigations in the performance of vehicle brake in order to improve their characteristics using 3-dimensions finite element technique. The technique of reduced householder and unsymmetric solver methods in the ANSYS 12 package will be used. Moreover, according to the review establishment, the present work outlines the mode shapes and natural frequencies of the brake disc and pads and their relation to contact stiffness and squeal. Therefore, this paper predicts the onset of brake squeal.

2. Finite element background and method of analysis

The finite element method is a technique for mathematically modelling complicated shapes (features) as an assembly of simpler shapes (elements) that is more easily defined. Linear and non-linear problems in brake field are of the great importance to be studied in this work. The meshed ventilated disc and friction materials are example of 3D finite elements models as shown in Figures 1 and 2. FEM (ANSYS) here is used to design the ventilated disc and the pad (friction material and back plate), efficiently and then these designs are split into elements (Brick elements). These elements are connected with each other through points called nodes. The complete collection of the elements is called mesh. Restraints and loads are added to the meshed part that is called model. The finite element technique has been used in this work to study the modal analysis of the ventilated disc, pad, coupled system (ventilated disc and pad). The modal analysis has been used to determine the vibration characteristics, which are natural frequencies and mode shapes of the coupled brake system which are very important in the design of any structure for dynamic loading conditions [39]. FEM technique can help in studying of brake squeal by determining the degree of instability from the complex eigenvalue analysis of the coupled system [37-44]. Modal analysis techniques can only be applied to a linear structural system that will be represented through Matrix 27 which has been chosen from the ANSYS 12 Package library. The geometry and material attributes of the components should be the same for each step in the package process of the modal analysis. The ventilated disc brake structure consisted of ventilated disc and two pads. Each pad consisted of back plate and friction material as shown in Figures 1 and 2. Solid 45 brick element was selected from the Ansys12 elements library, Element Library [40] to model the 3D solid structure. This element was defined by 8-nodes with three degrees of freedom for each node in the coordinates of X, Y and Z respectively.

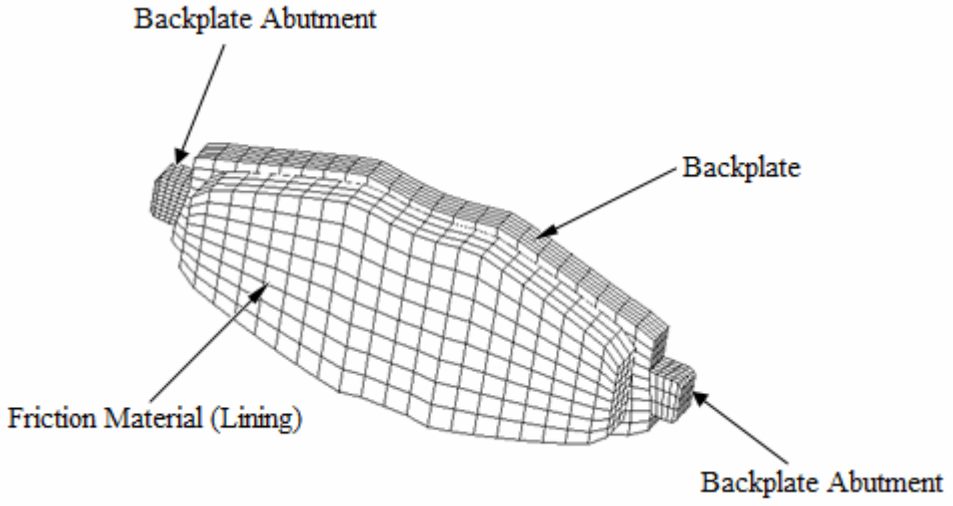

Figure 1. Layout of the meshed Pad

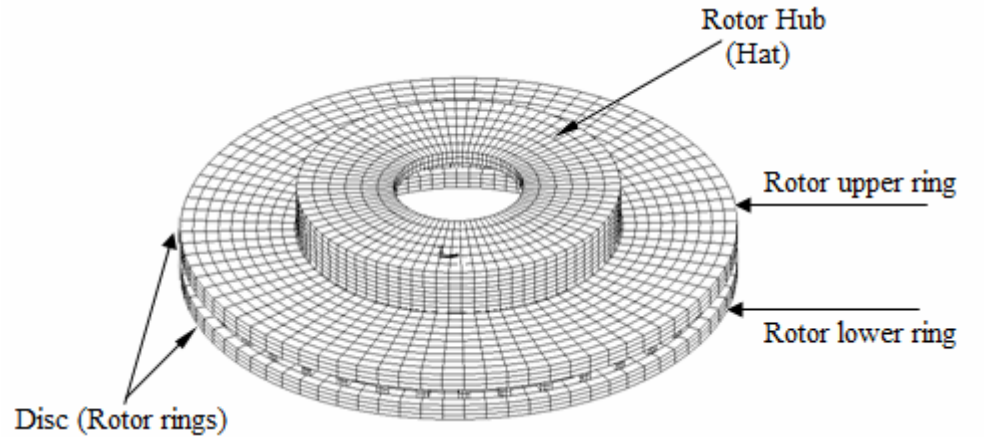

Figure 2. Layout of the meshed ventilated disc

3. Program validation

The modal analysis work herein of the ventilated disc and the pad was validated with 2 known models as of the experimental work of Fieldhouse and Newcomb [45], who studied modal analysis by using the holographic interferometery to the ventilated disc and pad. The second model is the theoretical work of Ribin [46] who used shell element STIFF63, [40]. However, the solid45 (Brick elements) has been chosen for this study. So, a rotor and pad with a similar specification as of [45, 46] were constructed. The boundary conditions such as constrained pad abutments and ventilated rotor inner periphery were applied to the chosen rotor and pad, and then the program solved the problem. Many trials were made to adjust the meshing for the rotor and the pad with the appropriate number of elements to reach the lowest difference between the experimental work, simple model and the used validated model in this study. Figure 3-a shows the relation between the rotor frequency and mode number for the experimental work, simplified model and the validated model. The Figure shows the maximum rotor frequency of the simplified model is 11225 Hz, which is 5.5% higher than the experimental work. The maximum rotor frequency of the validated model by Ansys12 is 2% higher than that of the experimental work. The validated model of the pad showed a maximum frequency difference of 7% lower than the experimental work, which was at the pad third mode. However, the theoretical model showed a maximum frequency difference of 12 % lower than the experimental. The difference between the experimental, theoretical and the validated model of the pad is shown in Figure 3-b.

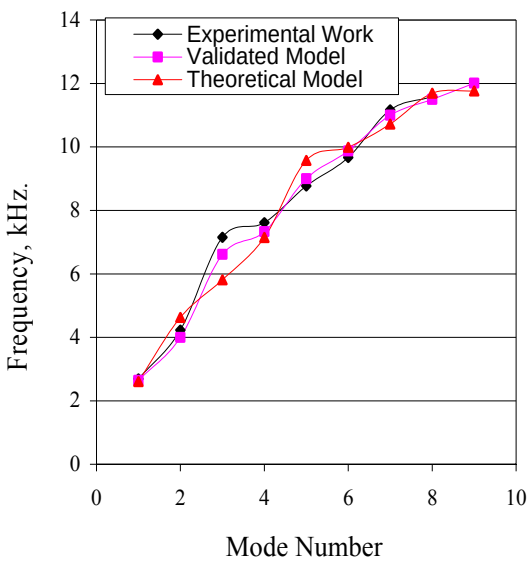

(a) Disc models

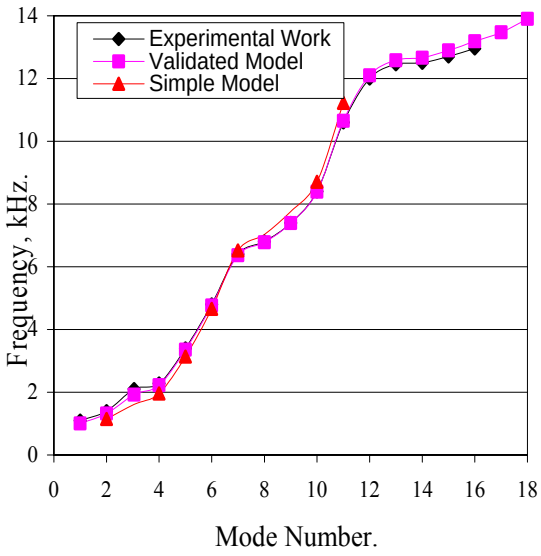

(b) Pad models

Figure 3. Comparison between the different models of the discs and for the pads respectively

4. Modeling of ventilated disc brake

The basic steps for performing a typical modal analysis Ansys 12 [41] are Pre-processor, solution and Postprocessors. The program pre-processor steps include creation of the model geometry and mesh. Then applying necessary boundary conditions and loads and defining solution options and load steps. Final step is to expand the modes and solving the problem and the postprocessor include reviewing the results. In this step, the geometry of the ventilated disc and the friction material was created. Choosing element types, real constant and material properties were very important for ANSYS 12 to apply the appropriate analysis. Meshing these surfaces by the suitable type of mesh as mapped or free. The mesh used in this work was the mapped mesh (brick meshing) by choosing solid45 element to simulate this type of brake, Modelling and Meshing Guide [42]. The mapped mesh has been chosen because it has restriction on the element shape while there was no restriction on the element shape in the case of free mesh. The model consisted of 8000 brick elements for the ventilated disc, 1110 brick elements for the backplate and 480 elements for the friction material as indicated in Figures 1 and 2.

5. Expanding the modes and substructure technique

The solution method during this work was the Reduced (Householder) method that uses the HBI (householder-Bisection-Inverse iteration) to calculate the eigenvalues and eigenvectors. It works with a small subset of degrees of freedom called master degrees of freedom (MDOF). Using these master degrees of freedom leads to an exact [K] matrix but an approximate [M]. Expanding of the modes meant expanding the reduced solution to the full DOF set. It applies not just to reduce mode shapes from the reduced mode extraction method, but to full mode shapes from the other mode extraction methods as well. However, substructuring technique was a procedure that condensed a group of finite elements into one element represented as a matrix. In a nonlinear analysis, the linear portion of the model was substructed so that the element matrices for that portion did not need recalculation every equilibrium iteration. In 3D cases (disc brake), the substructures contained three rigid body rotations and three translational motions. It simply represents a collection of elements that are reduced to act as one element. This one (super) element may then be used in the actual analysis or be used to generate more superelements. In a static problem, the equation of the finite element is reduced to be in the form of:

$$[K]\{u\} = \{F\} \tag{1}$$

where:
[K]: is the element stiffness matrix, {u}: is the vector representing the total degrees of freedom, {F}: is the force vector.

Selecting active degrees of freedom, which were also known as master degrees of freedom that denoted by subscript m, while the remaining degrees of freedom were considered as slave degrees of freedom that denoted by subscript s, can reduce the problem, Theory Manual [44]. The stiffness matrix was partitioned into sub matrices according to master and slave degrees of freedom as follows:

$$\begin{bmatrix} [K_{mm}] & [K_{ms}] \\ [K_{sm}] & [K_{ss}] \end{bmatrix} \begin{Bmatrix} \{u_m\} \\ \{u_s\} \end{Bmatrix} = \begin{Bmatrix} \{F_m\} \\ \{F_s\} \end{Bmatrix} \tag{2}$$

It was arranged so that {Fs} = 0 i.e. external forces were applied at master degrees of freedom only. Expanding equation (3) so that:

$$[K_{mm}]\{u_m\} + [K_{ms}]\{u_s\} = \{F_m\} \tag{3}$$

$$[K_{sm}]\{u_m\} + [K_{ss}]\{u_s\} = \{F_s\} \tag{4}$$

Solving for the slave degrees of freedom in equation (4)

$$\{u_s\} = [K_{ss}]^{-1}\{F_s\} - [K_{ss}]^{-1}[K_{sm}]\{u_m\} \tag{5}$$

Finally by substituting equation (5) into equation (3), then

$$\left[[K_{mm}] - [K_{ms}][K_{ss}]^{-1}[K_{sm}]\right]\{u_m\} = \{F_m\} - [K_{ms}][K_{ss}]^{-1}\{F_s\} \tag{6}$$

Or

$$[\hat{K}]\{\hat{u}\} = \{\hat{F}\} \tag{7}$$

Where

$$[\hat{K}] = [K_{mm}] - [K_{ms}][K_{ss}]^{-1}[K_{sm}] \tag{8}$$

And

$$\{\hat{u}\} = \{u_m\} \tag{9}$$

And

$$\{\hat{F}\} = \{F_m\} - [K_{ms}][K_{ss}]^{-1}\{F_s\} \tag{10}$$

The same method was extended to dynamic analysis:

$$[\hat{M}]\{\hat{\ddot{u}}\} + [\hat{C}]\{\hat{\dot{u}}\} + [\hat{K}]\{\hat{u}\} = \{\hat{F}\} \tag{11}$$

Where, by using Guyan's reduction technique, Guyan [47] for the mass reduction:

$$[\hat{M}] = [M_{mm}] - [K_{ms}][K_{ss}]^{-1}[M_{sm}] - [M_{ms}][K_{ss}]^{-1}[K_{sm}] + [K_{ms}][K_{ss}]^{-1}[M_{ss}][K_{ss}]^{-1}[K_{sm}] \tag{12}$$

The terms derived for the reduced mass, damping, stiffness and force matrices were also known as the superelement coefficients, since in the finite element method, the technique of reducing a component matrix was akin to forming a superelement with its own mass, damping, and stiffness matrices. The reduced stiffness matrix was said to be complete since all the elements of the original stiffness matrices contributed as shown in equation (8). In the case of reduced mass matrix, combinations of stiffness and mass element appeared. As a result, the completeness in the eigenvalue-eigenvector problem was said to be closely but not exactly preserved.
And by applying this substructure technique to solve the eigenvalue problem which was in the form of:

$$\left[\left[\hat{K}\right]-\omega^2\left[\hat{M}\right]\right]\{\hat{u}\}=\{0\} \tag{13}$$

It led to:

$$\left[\begin{bmatrix}[K_{mm}] & [K_{ms}]\\ [K_{sm}] & [K_{ss}]\end{bmatrix}-\omega^2\begin{bmatrix}[M_{mm}] & [M_{ms}]\\ [M_{sm}] & [M_{ss}]\end{bmatrix}\right]\cdot\begin{Bmatrix}\{u_m\}\\ \{u_s\}\end{Bmatrix}=\begin{Bmatrix}\\ 0\\ \\ \end{Bmatrix} \tag{14}$$

The Ansys 12 program started to solve this problem by the Reduced Housholder solver to get the eigenvalue and eigenvectors of the ventilated disc and pad separately.

6. Modal analysis of the coupled ventilated disc brake system

Brake squeal phenomenon involved modal coupling between various modes. In order to reduce or eliminate this squeal, it was very important to the coupling mechanism to be understood very well. This piece of work dealt with the coupled ventilated disc brake system through studying the mode shape of the coupled system. The technique used here in this study was investigating modal coupling using the complex eigenvalue method, Unsymmetric solver [43] to analyse mode shapes associated with the predicted natural frequency. Creating the element of Matrix27 between the ventilated disc and pad was very important in studying the squeal of the coupled ventilated disc brake. Studying the mode shape of the coupled rotor and pads was of great importance in predicting the squeal that happened during this coupling. The eigenvalues of the coupled system were in the form of complex numbers. Complex numbers contained mainly two parts; the first part was the real part while the second was the imaginary part. The imaginary part in this particular solver gave a measure to the instability of the system while the real part gave the frequency of the system. The geometry used in this modal analysis technique for the coupled system consisted of the rotor and two pads (inboard and outboard). Each pad also consisted of two parts, the friction material and the backplate as shown in Figure 4. The pad length was 96 mm that covered an angle equal to 60 degree of the ventilated disc, which had a diameter of 214 mm. To use the unsymmetric solver of the modal analysis, the stiffness matrix element Matrix27 should be created between the rotor and the pad (coupling equation) to obtain the natural frequency and mode shape of the system. So, the squeal intensity (propensity) can be evaluated from the magnitude of the instability measurements over the frequency range of interest. The unsymmetric method, which also uses the full [K] and [M] matrices, is meant for problems where the stiffness and mass matrices are unsymmetric. It uses Lanczos algorithm, [44] that calculate complex eigenvalues and eigenvectors for any system. In this particular case, the real part of the eigenvalue represented the natural frequency and the imaginary part was a measure of the stability of the system that a negative value of the imaginary part meant the system was stable while the positive value meant the system was unstable.
Matrix27 represented an arbitrary element whose geometry was undefined but whose elastic kinematics response could be specified by stiffness, damping, or mass coefficients. This element matrix27 was assumed to relate two nodes, each with six degrees of freedom per node: translations in the nodal x, y, and z directions and rotations about the nodal x, y, and z-axes. All matrices generated by this element were 12 by 12. The degrees of freedom were ordered as UX, UY, UZ, and ROTX, ROTY, ROTZ for node I followed by the same for node J. If one node was not used, so all rows and columns related to this node would be defaulted to zero. The node location and the coordinate system for this element are shown in Figure 5.

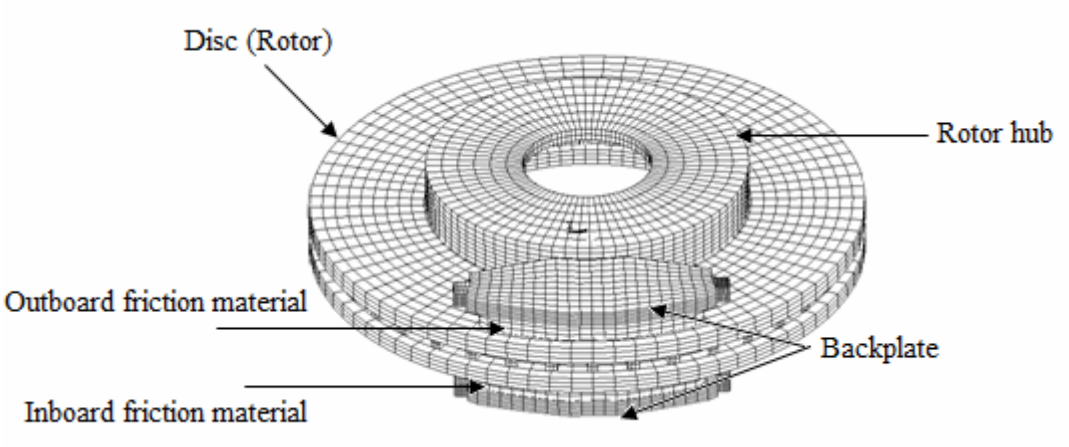

Figure 4. Finite element model for the coupled ventilated disc brake

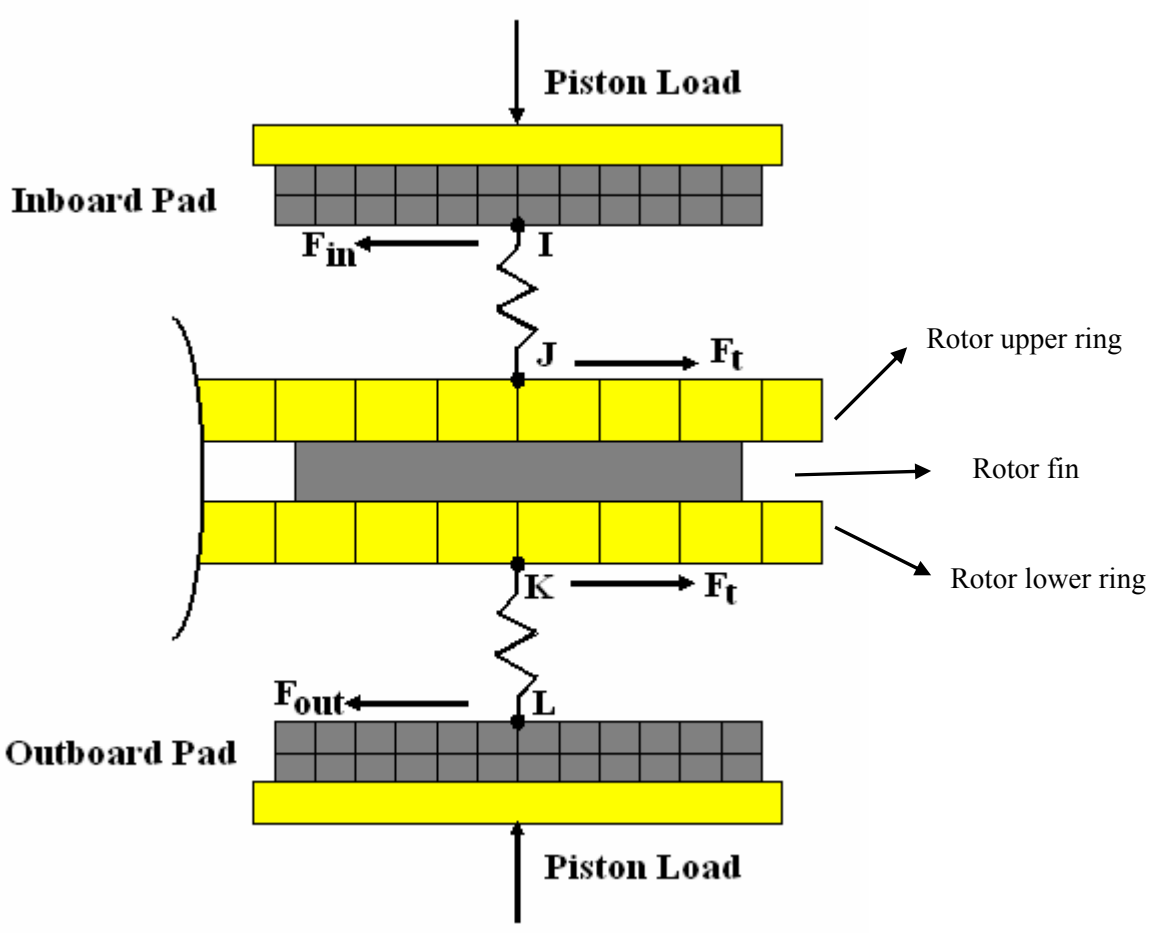

Figure 5. Linear representation of the coupled ventilated disc brake

For most brake design, including this study, there was no viscous damping present. According to the geometric instability, variable frictional forces, due to variable normal forces, caused brake squeal to occur [11]. The matrix equation of motion in the absence of viscous damping and including the frictional forces was:

$$[M]\{\ddot{U}\} + [K]\{U\} = \{F_f\} \quad (15)$$

To allow variable normal forces at the rotor-lining interface, adjacent nodes on the rotor and lining were connected together with stiff spring as shown in Figure 5. Since squeal typically occurred at low applying pressures, a constant contact pressure was assumed between both friction material surface and the rotor surface [11, 15]. As the connected nodes moved towards or away from each other, the magnitude of the normal force increased or decreased according to moving direction. So, the resulting variable frictional forces were written in terms of relative displacement between the mating surfaces.

$$\{F_f\} = [K_f]\{U\} \tag{16}$$

This matrix, which related the frictional forces to nodal displacement called the frictional stiffness matrix $[K_f]$or the friction matrix. To obtain a homogeneous equation, the forces were moved from the right side of equation (15) to the left side of the same equation to be in the form of;

$$[M]\{\ddot{U}\} + [K - K_f]\{U\} = 0 \tag{17a}$$

The complementary solution of equation (17) could be written in the form of:

$$\{U\} = \{\phi\}e^{st} \tag{17b}$$

where:
s: is the eigenvalue, $\{\phi\}$ is the eigenvector.

And by substitution in equation (16) So;

$$([M]S^2 + [K - K_f])\{\phi\} = \{0\} \tag{18}$$

The eigenvalue and possibly the eigenvectors of equation (18) were complex numbers. Complex numbers contained two parts; real and imaginary parts. For this ventilated disc brake system, the eigenvalues always occurred in complex conjugate pairs. For certain mode, the eigenvalue was:

$$S = \sigma_i \pm j\omega_i \tag{19}$$

where:
σ_i: is the real part and represented the natural frequency of the system, ω_i: is the imaginary part and represented the instability of the system.

Nodes I and J were the two-node system represented the upper contact between the inboard pad and the rotor (upper ring). It was realized the spring between I and J compressed only in the Z-direction while was not allowed for any other displacement in the X or Y-directions. Also, nodes K and L were the two-node system represented the lower contact between the outboard pad and the rotor (lower ring) as clear in Figure 5. The frictional interface behaviour over the piston loaded interface was given by the equations mentioned earlier and could be represented by an unsymmetric stiffness matrix $[K_f]$ that coupled I and J contact nodes in six degrees of freedom as follows:

$$\{Ff\} = [K_f]\{U\} \tag{20}$$

where:
{Ff}: denotes the unsymmetric interfacial force vector, $[K_f]$: denotes the unsummetric interfacial stiffness matrix, {U}: denotes the nodal displacement vector, M: denotes the moment about x,y and z axis exerted at each contact point.

$$\begin{bmatrix} F_{XI} \\ F_{YI} \\ F_{ZI} \\ M_{XI} \\ M_{YI} \\ M_{ZI} \\ F_{XJ} \\ F_{YJ} \\ F_{ZJ} \\ M_{XJ} \\ M_{YJ} \\ M_{ZJ} \end{bmatrix} = \begin{bmatrix} C_1 & C_2 & C_3 & C_4 & C_5 & C_6 & C_7 & C_8 & C_9 & C_{10} & C_{11} & C_{12} \\ C_{79} & C_{13} & C_{14} & C_{15} & C_{16} & C_{17} & C_{18} & C_{19} & C_{20} & C_{21} & C_{22} & C_{23} \\ C_{80} & C_{81} & C_{24} & C_{25} & C_{26} & C_{27} & C_{28} & C_{29} & C_{30} & C_{31} & C_{32} & C_{33} \\ C_{82} & C_{83} & C_{84} & C_{34} & C_{35} & C_{36} & C_{37} & C_{38} & C_{39} & C_{40} & C_{41} & C_{42} \\ C_{85} & C_{86} & C_{87} & C_{88} & C_{43} & C_{44} & C_{45} & C_{46} & C_{47} & C_{48} & C_{49} & C_{50} \\ C_{89} & C_{90} & C_{91} & C_{92} & C_{93} & C_{51} & C_{52} & C_{53} & C_{54} & C_{55} & C_{56} & C_{57} \\ C_{94} & C_{95} & C_{96} & C_{97} & C_{98} & C_{99} & C_{58} & C_{59} & C_{60} & C_{61} & C_{62} & C_{63} \\ C_{100} & C_{101} & C_{102} & C_{103} & C_{104} & C_{105} & C_{106} & C_{64} & C_{65} & C_{66} & C_{67} & C_{68} \\ C_{107} & C_{108} & C_{109} & C_{110} & C_{111} & C_{112} & C_{113} & C_{114} & C_{69} & C_{70} & C_{71} & C_{72} \\ C_{115} & C_{116} & C_{117} & C_{118} & C_{119} & C_{120} & C_{121} & C_{122} & C_{123} & C_{73} & C_{74} & C_{75} \\ C_{124} & C_{125} & C_{126} & C_{127} & C_{128} & C_{129} & C_{130} & C_{131} & C_{132} & C_{133} & C_{76} & C_{77} \\ C_{134} & C_{135} & C_{136} & C_{137} & C_{138} & C_{139} & C_{140} & C_{141} & C_{142} & C_{143} & C_{144} & C_{78} \end{bmatrix} \times \begin{bmatrix} X_I \\ Y_I \\ Z_I \\ \theta_{XI} \\ \theta_{YI} \\ \theta_{ZI} \\ X_J \\ Y_J \\ Z_J \\ \theta_{XJ} \\ \theta_{YJ} \\ \theta_{ZJ} \end{bmatrix}$$

Thus, the stiffness matrix27 was in the form as indicated previously by Ansys (39, 40, 51 – 56), where for the two-node system I and J as clear in Figure 5 that:

$C3 = C60 = -C9 = -C96 = \mu \times \sin\theta \times K_C$

$C14 = C65 = -C20 = -C102 = \mu \times \cos\theta \times K_C$

$C24 = C69 = -C30 = -C109 = K_C$ and the missing C are zeros.

And for the two-node system K and L as in Figure 5 that:

$C3 = C60 = -C9 = -C96 = -\mu \times \sin\theta \times K_C$

$C14 = C65 = -C20 = -C102 = -\mu \times \cos\theta \times K_C$

$C24 = C69 = -C30 = -C109 = K_C$ and the missing C are zeros.

The two unsymmetric stiffness matrices were calculated for the linear interfacial elements inserted between the two linings and the ventilated disc to simulate the frictional interface mechanism. Then, a linear modal analysis could be performed to extract the complex eigenvalues for the prediction of the dynamic response of the ventilated disc brake system.

7. Determining contact stiffness

Any coupling problems require stiffness between the two contact surfaces. The amount of penetration between the disc and pad depends on this stiffness. Higher stiffness values could lead to ill conditioning of the stiffness matrix and to convergence difficulties. Ideally, a high enough stiffness wanted that contact penetration was acceptably small, but a low enough stiffness that the problem could be well behaved in terms of convergence or matrix ill conditioning and might cause excessive penetration. FE programs employed a contact stiffness to enforce compatibility between two contacting nodes at material interface. The value of this contact stiffness controlled the accuracy of the contact behaviour as well as the convergence characteristics of the problem Ansys 12 [44]. Therefore, appropriate contact stiffness must be determined before commencement of the main simulation program of works.

In the basic Coulomb friction model, two contacting surfaces could carry shear stresses up to a certain magnitude across their interface before they start sliding relative to each other. This state was known as sticking. The Coulomb friction model defined as an equivalent shear stress τ at which sliding on the surface began as a fraction of the contact pressure P ($\tau = \mu . P$). Once the shear stress exceeded, the two surfaces slid relative to each other, this state was known as sliding. For most contact analysis, the normal contact stiffness K_C could be estimated as follows:

$$K_C = f.E.h \tag{21}$$

where:

f: is a constant value ranging from 0.01 to 10 [44], E: is the Young's Modulus (if there are two contact surfaces with different materials, the smaller value is E and it was taken for the pad), H: is characteristic contact length (it was taken as a pad length=106 mm).

Determining a good stiffness value required some experimentation on the model and to arrive at a good stiffness value. Many trials were made between 0.01 and 10 for the value of f to get the appropriate contact stiffness and it was found to be 1000 MN/m2. In general, it was better to underestimate this value rather than overestimate it.

8. Results and discussions

8.1 The ventilated rotor

The eigenvalue analysis of the ventilated rotor shown in Figure 2 gave 100 modes in the frequency range of 1-15 kHz including a number of nodal lines ranging 1- 7 nodal lines (diametral modes) as clearly shown in Figures 6 and 7. It showed samples of rotor modes layout and the displacement contours of the disc indicating the maximum and minimum ventilated rotor displacements that occurred at the different mode frequencies. The distribution of the contour in these Figures had nine lines starting with letter A and ending with letter I, however the letter E was in the middle of the contour that considered being zero displacement. Letter A showed the maximum displacement in the z-direction while letter I showed the maximum displacement in the opposed z-direction to that of letter A, which called anti-nodal displacement. However, letter E showed the minimum (zero or close to zero displacement that called the nodal lines or nodes.

It is realized from the analysis that the first mode occurred at frequency of 1019 Hz as shown in Figure 6(a, b, c, d, e and f). The first mode contained 6 nodal lines (diametral lines and a maximum displacement of 0.7 mm without any circumferential lines which is clear in Figure 7-a. However, the third mode of frequency 1176 Hz showed four nodal lines and zero circumferential lines. It appeared on the upper ring of the ventilated rotor with a maximum displacement of 2.8 mm as shown in Figures 6-a and 7-b. Figures 6-b and 7-c showed the 25^{th} mode that occurred at frequency 1391 Hz which contained 7 nodal lines on the lower ring of the rotor with a maximum displacement of 2.4 mm and there was no any circumferential lines appeared through this mode. The 33^{rd} mode happened at frequency of 1500 Hz. It showed 4 nodal lines on the upper ring of the rotor and 1 nodal line on the hub of the rotor which is clear enough in Figures 6-c and 7-d. It showed a maximum displacement of 1.3 mm on the upper ring of the rotor however, it was 0.33 mm on the rotor hub. The 35^{th} mode happened at frequency of 1548 Hz. It showed 7 nodal lines on the lower ring of the rotor and there was no nodal line appeared through this mode on the hub of the rotor which is clear in Figures 7-e. It showed a maximum displacement of 1.7 mm on the lower ring of the rotor.

The 38^{th} mode occurred at frequency of 1634 Hz as clear in Figures 6-d and 6-e. It showed 6 nodal lines on the lower ring of the rotor and also there was no nodal line on the hub of the rotor. There were six maximum displacements of 1.4 mm marked with letter I and also eight minimum displacement of marked with letter E to indicate the fourth diametral mode that occurred at frequency of 2703 Hz that occurred at the 79^{th} mode. However, the 80^{th} mode that occurred at frequency of 2716 Hz as shown clearly in Figures 6-f and 7-f. This mode showed a number of maximum and minimum displacements to confirm that mode of the second diametral mode. A maximum displacement of 1.5 mm was observed on the upper ring of the rotor.

8.2 The pad

The modal analysis of the pad (friction material and backplate) has been also studied by using the FE of Ansys12 package. The pad consisted of two parts; the first part was the backplate that was made of mild steel while the second part was the friction material. The eigenvalue analysis of the pad shown in Figure 1 gave 69 modes in the frequency range of 1-15 kHz including nodal lines (diametral modes) and anti-nodal lines. The pad eigenvalues were calculated using the Reduced (Householder Method) solver [40] as the same technique for the ventilated rotor. The first mode occurred at frequency of 1067 Hz, which was of the first twisting mode types as shown in Figure (8-a). Figure 8 (a, b, c, d, e and f) shows a sample of 6 modes of the 69 modes of the pas showing the 1^{st}, 2^{nd}, 3^{rd}, 7^{th}, 10th and 39^{th} mode of the pad. It can be seen from these figures that the second mode also was a bending mode type but for the backplate. The third mode happened at frequency of 1424 Hz as seen in Figure 8-c, which was also bending mode as known that the modes of the pad during the study of the mode shape generally contained two types of modes, which were bending and twisting mode and in some cases, it could be a mixed of bending and twisting modes.

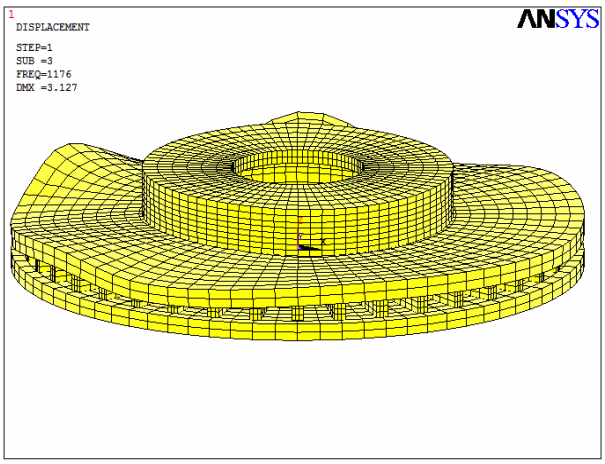

(a) Frequency 1176 Hz

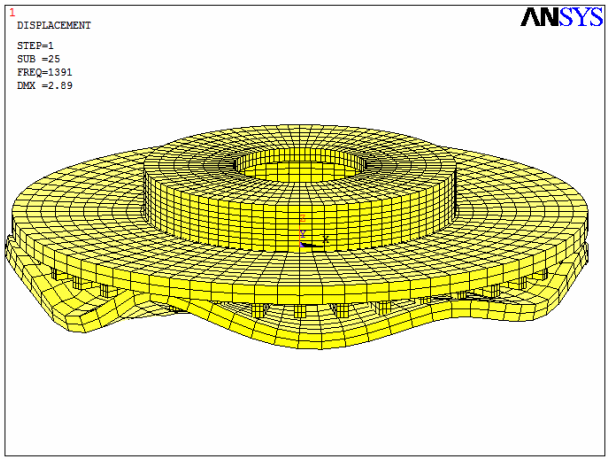

(b) Frequency 1391 Hz

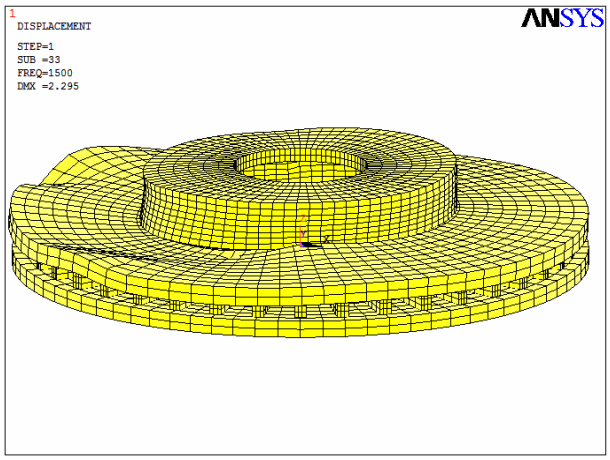

(c) Frequency 1500 Hz

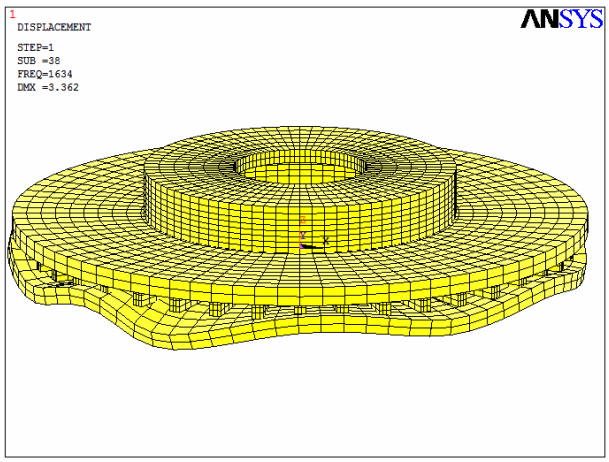

(d) Frequency 1634 Hz

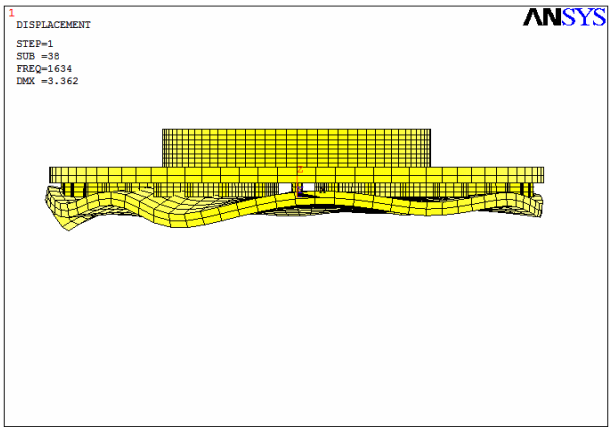

(e) Frequency 1634 Hz

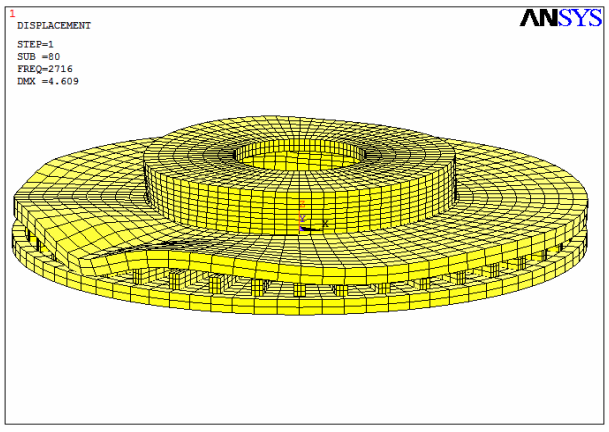

(f) Frequency 2716 Hz

Figure 6. Ventilated rotor modes 3, 25, 33, 38 and 80th respectively

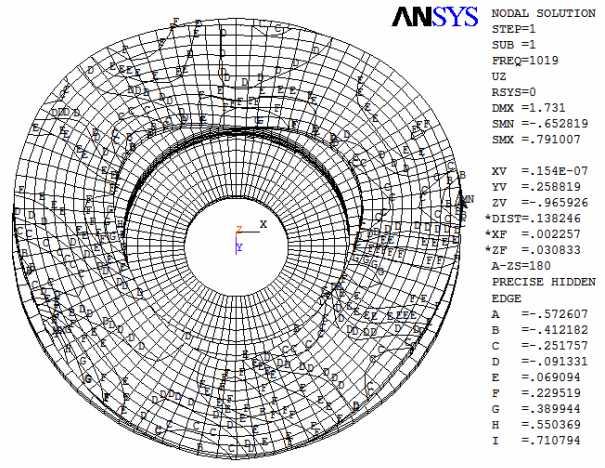

(a) Frequency 1019 Hz

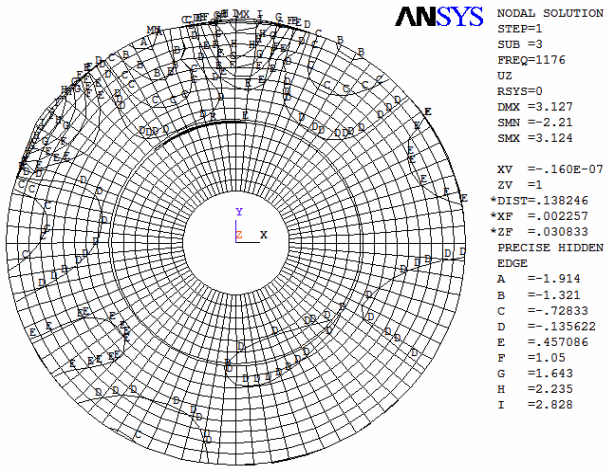

(b) Frequency 1176 Hz

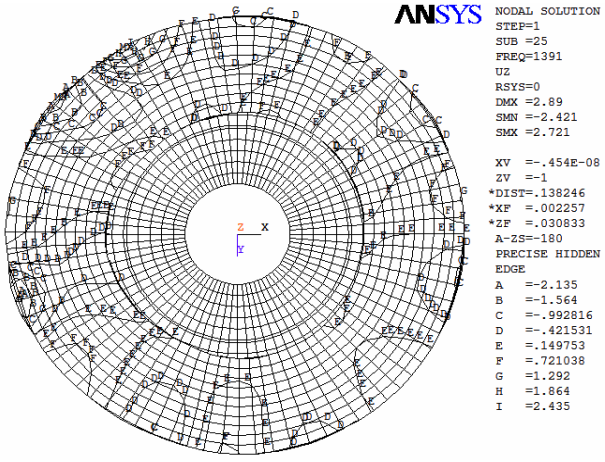

(c) Frequency 1391 Hz

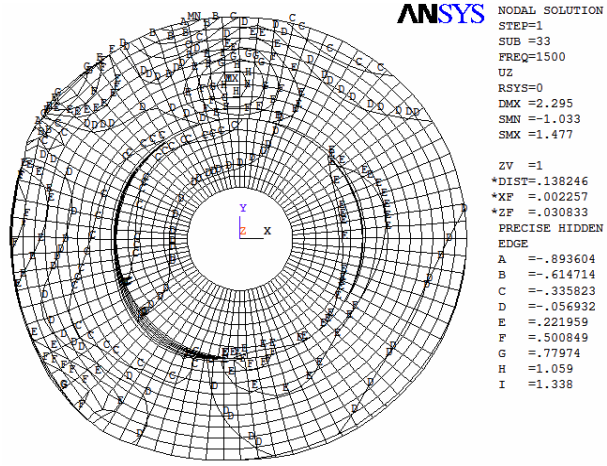

(d) Frequency 1500 Hz

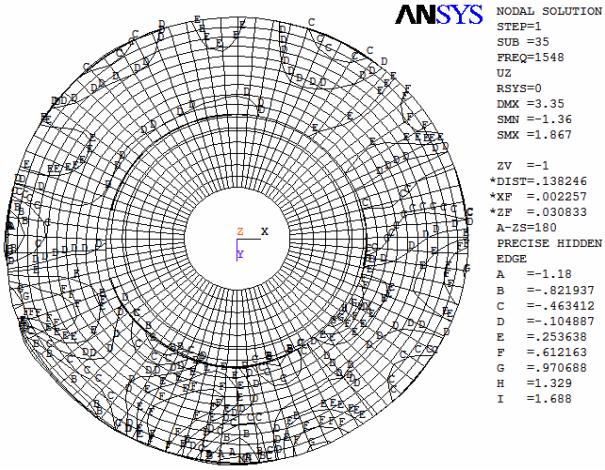

(e) Frequency 1548 Hz

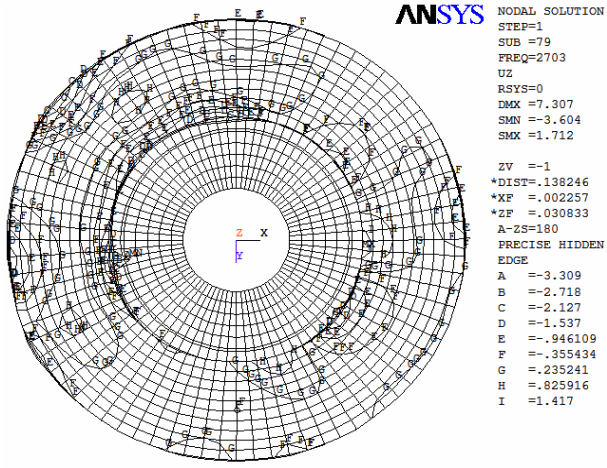

(f) Frequency 2703 Hz

Figure 7. Displacement contours at modes 1, 3, 25, 33, 35 and 79th respectively

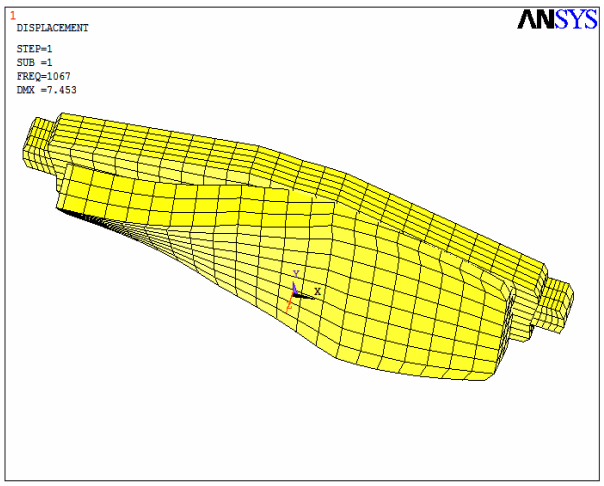

(a) Frequency 1067 Hz

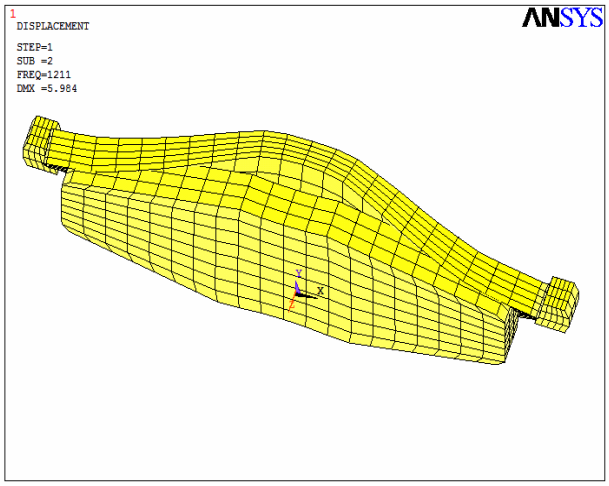

(b) Frequency 1211 Hz

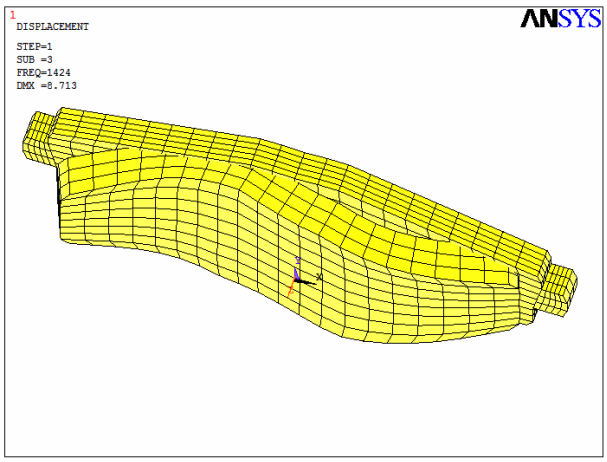

(c) Frequency 1424 Hz

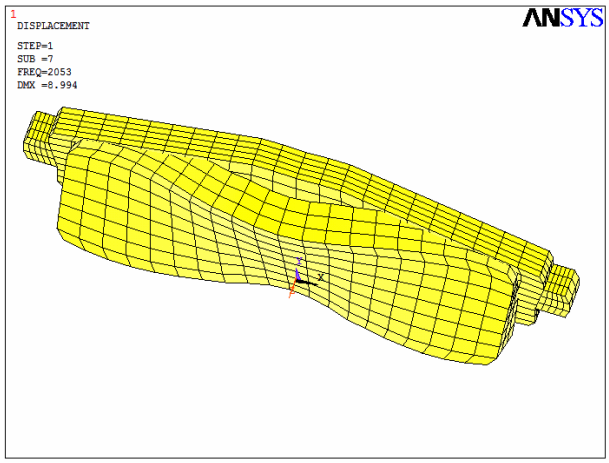

(d) Frequency 2053 Hz

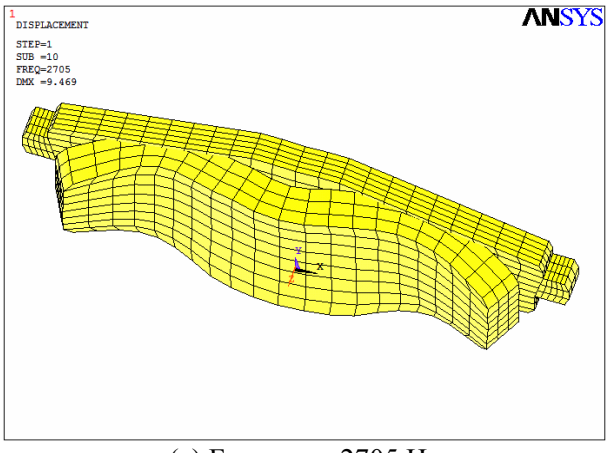

(e) Frequency 2705 Hz

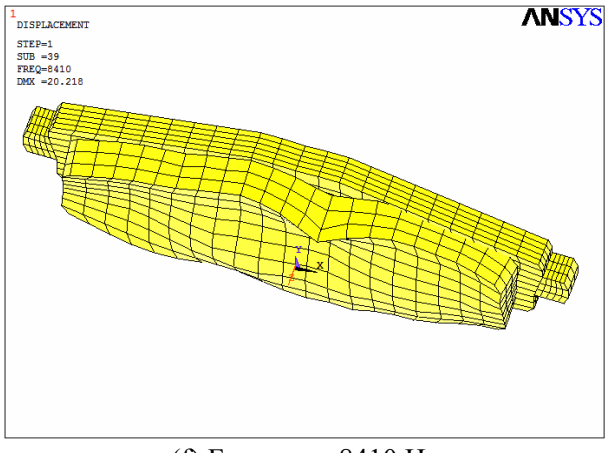

(f) Frequency 8410 Hz

Figure 8. Pad modes 1, 2, 3, 7, 10 and 39th respectively

The equal displacement contour plot samples of modes 2, 4, 6, 14, 24 and 32 that occurred at frequencies of 1211, 1612, 1928, 3196, 4820 and 6907 Hz respectively are clearly shown in Figure 9 (a, b, c, d, e and f). These Figures show a number of nodal lines different from 2nd mode till 32nd mode indicating 9 lines of different displacements starting with letter A and ending with letter I. Letter A shows the maximum displacement in the Z-direction however letter I shows the maximum displacement in the opposite Z-direction that called the minimum displacement of the mode (or vice versa). It shows a mix of the bending modes, twisting modes or combined of bending and twisting modes. The number of the nodal

lines in these Figures starting from 2 nodal lines till 7 nodal lines which is very clear through the nine letters that are located on the right of the Figures.

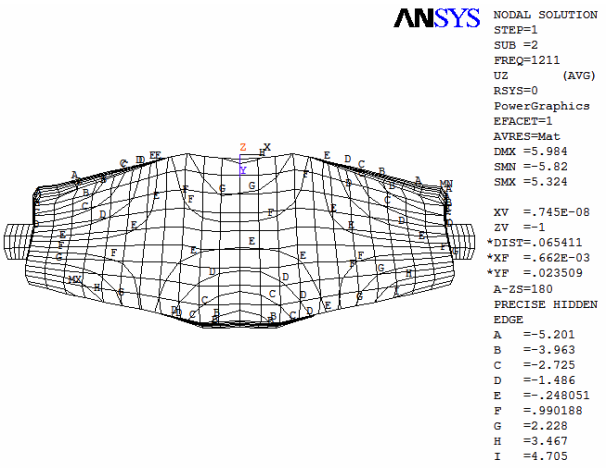

(a) Frequency 1211 Hz

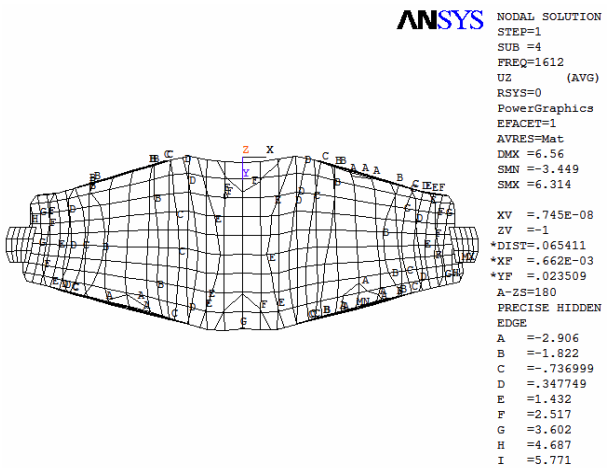

(b) Frequency 1612 Hz

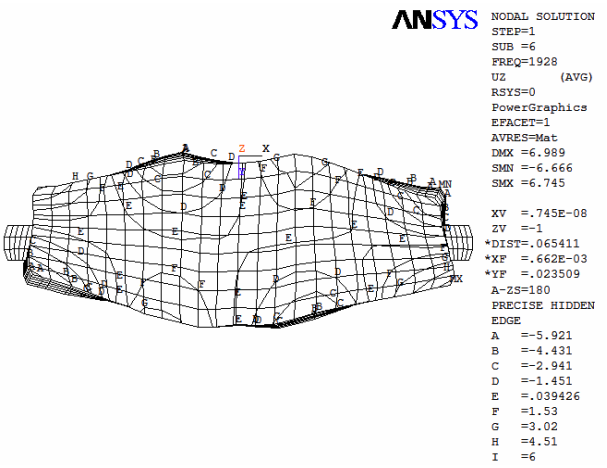

(c) Frequency 1928 Hz

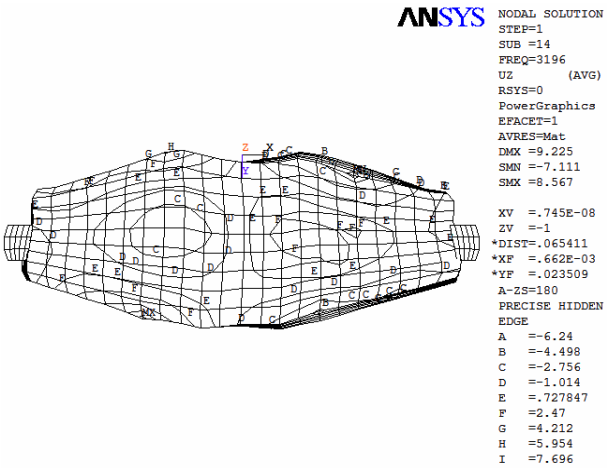

(d) Frequency 3196 Hz

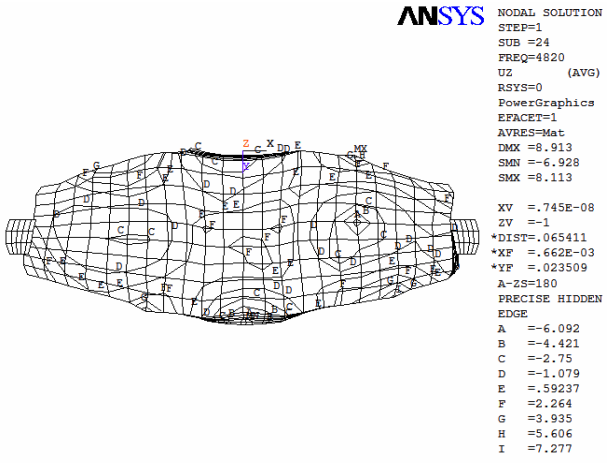

(e) Frequency 4820 Hz

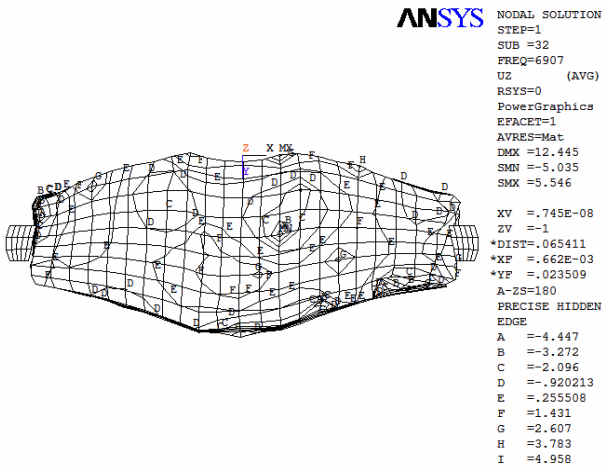

(f) Frequency 6907 Hz

Figure 9. Displacement contours at modes 2, 4, 6, 14, 24 and 54th respectively

8.3 The coupled disc brake system

Figures 10 and 11 show samples of the 28 modes of the coupled brake system in this squeal frequency range of 1-15 kHz that containing normal and complex modes. The modes were classified into two

categories; the first category was the normal mode that contained zero imaginary part and the second category was the complex mode that contained both real and imaginary parts through this particular "Unsymmetric" solver. The imaginary part of the complex mode could be either positive value, which meant the system, was instable or negative value, which meant the system, was stable. It was realized from the analysis that complex modes were conjugate as mentioned previously. The maximum imaginary part (instability reached during this study was 480 sec^{-1} recorded at frequency of 4083 Hz that represented the 16^{th} mode. The minimum imaginary part (instability was 0.02 sec^{-1} recorded at frequencies of 1035 and 1647 Hz, which represented mode numbers of 1 and 5. Mode 16^{th} represented the two-conjugate pair of complex mode oscillating at the same frequency of 4083 Hz. The real parts of the two modes are identical with the same sign because it represents the natural frequency of the mode; however the imaginary part of the same mode is illustrated in Figure 10-h. It can be seen also from those Figures that the pattern of the real part contained 4 nodal lines on the upper ring of the disc surface and there was no nodal lines observed on either the lower ring of the disc brake rotor or the rotor hub surface and also there were no nodal circles (circumferential lines observed on this mode. The phase angle of this mode was 3°, which equal to $Tan^{-1}\left(\frac{\text{Im } ag \text{ . Part}}{\text{Re } al \text{ Part}}\right)$, [37]. Mode 14^{th} occurred at frequency of 3440 Hz as seen in Figure 11-e, which represented the modes with one of the smallest imaginary part of 0.03. It was also realized that the real parts of the two modes were identical and the imaginary parts of the same modes were also identical but with different sign. There were three nodal lines observed on the upper ring of ventilated rotor surface and zero nodal lines on the disc hub. There were also zero nodal circles on both disc surface and disc hub. It also shows the oscillating inboard pad with the bending mode type. It was realized the two imaginary parts were the same just in the layout of mode but had a phase difference of 180°. There were no nodal lines observed on either the rotor rings or rotor hub and there was just displacement of 0.03 mm observed 3 times on the upper ring of the rotor.

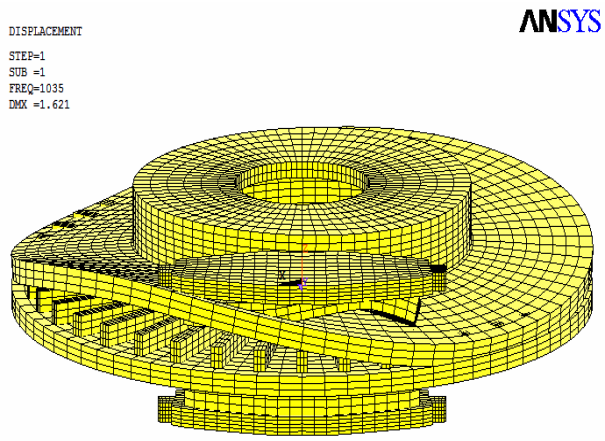

(a) Frequency 1035 Hz

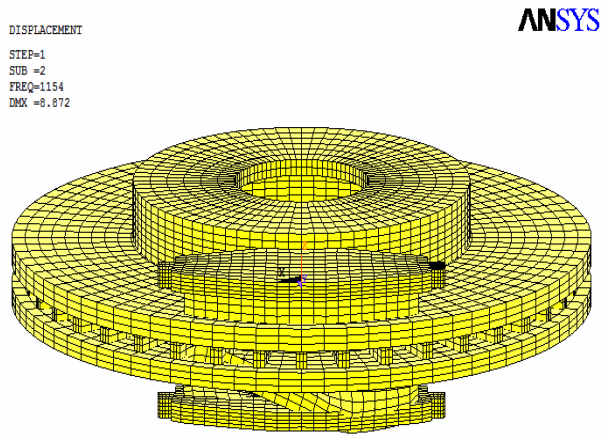

(b) Frequency 1154 Hz

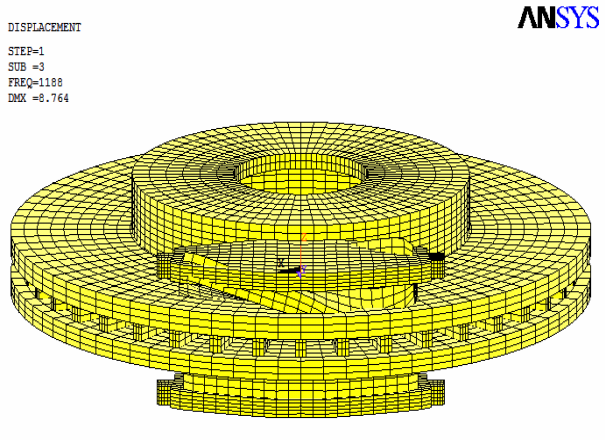

(c) Frequency 1188 Hz

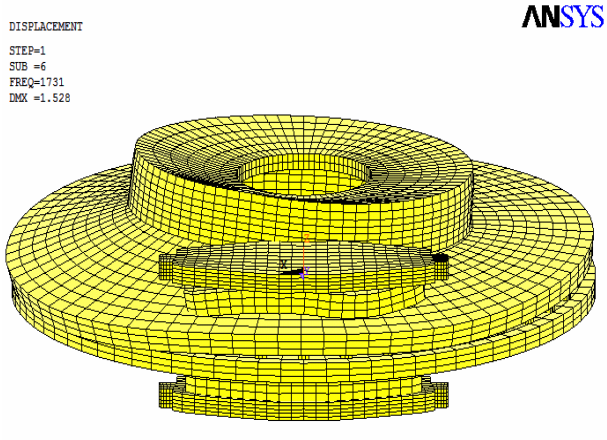

(d) Frequency 1731 Hz

Figure 10. (Continued)

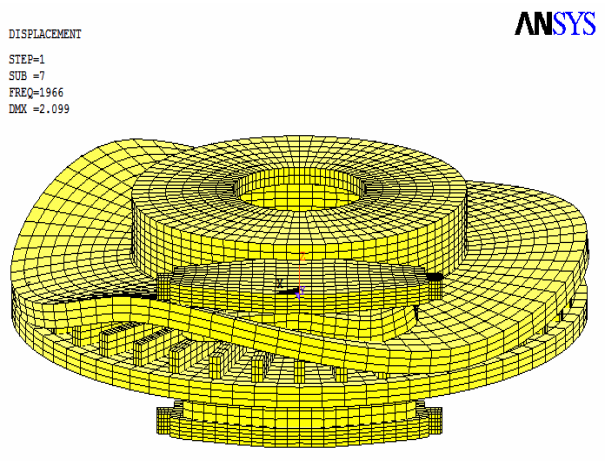

(e) Frequency 1966 Hz

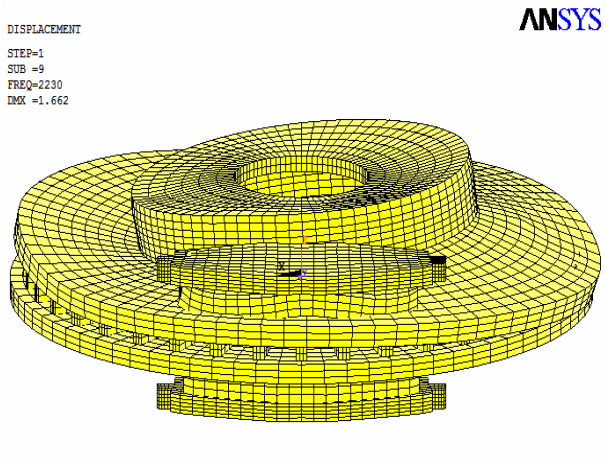

(f) Frequency 2230 Hz

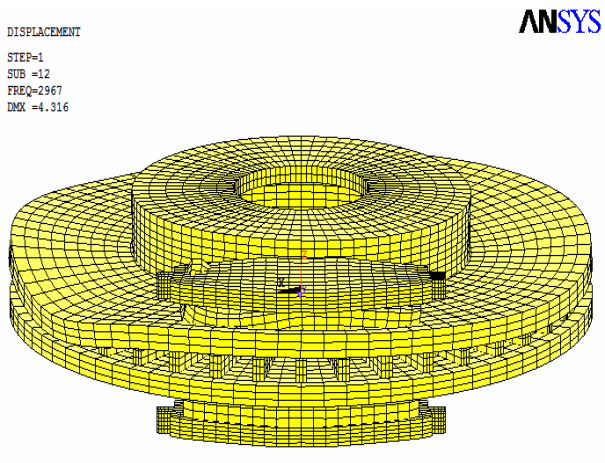

(g) Frequency 2967 Hz

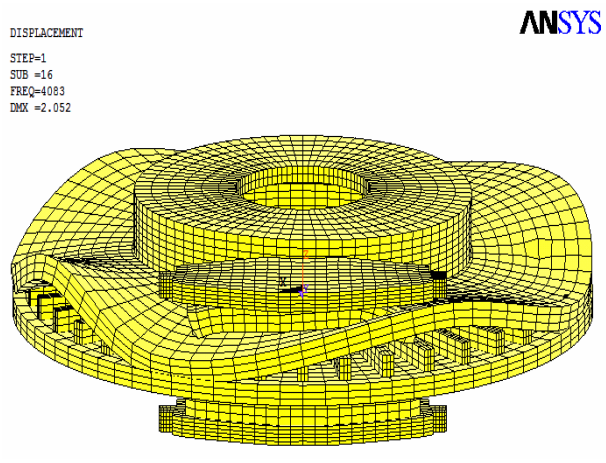

(h) Frequency 4083 Hz

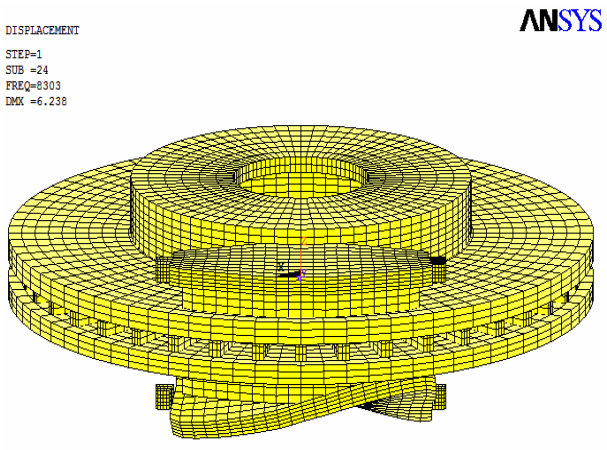

(i) Frequency 8303 Hz

Figure 10. Coupled ventilated disc brake modes 1, 2, 3, 6, 7, 9, 12, 16 and 24th respectively

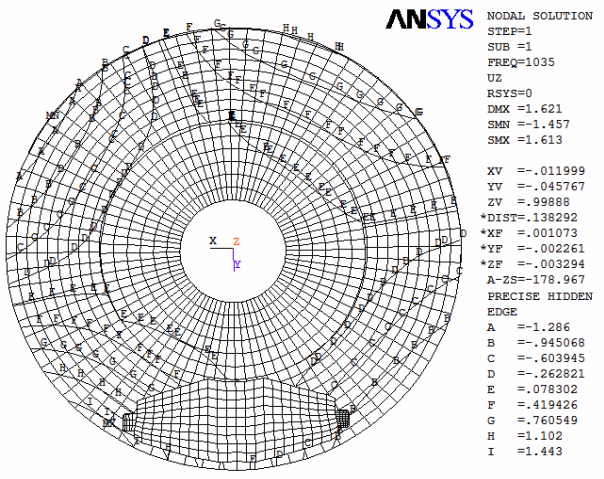

(a) Frequency 1035 Hz

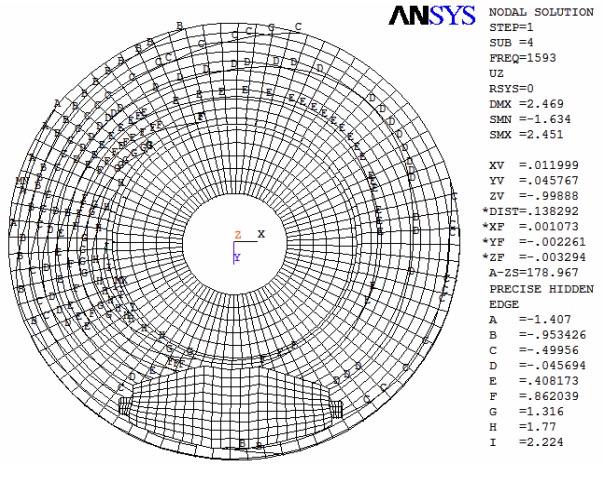

(b) Frequency 1593 Hz

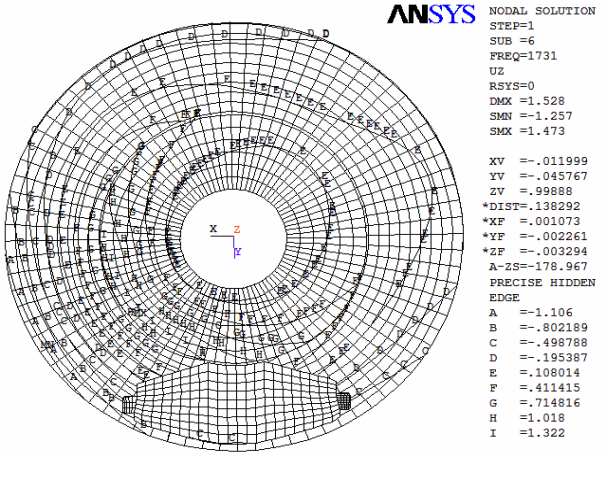

(c) Frequency 1731 Hz

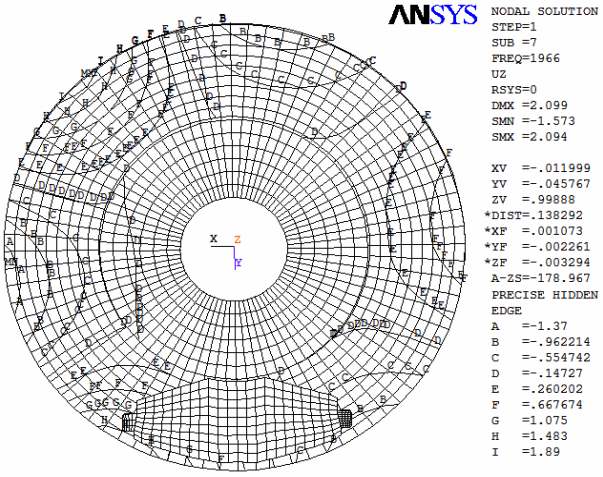

(d) Frequency 1966 Hz

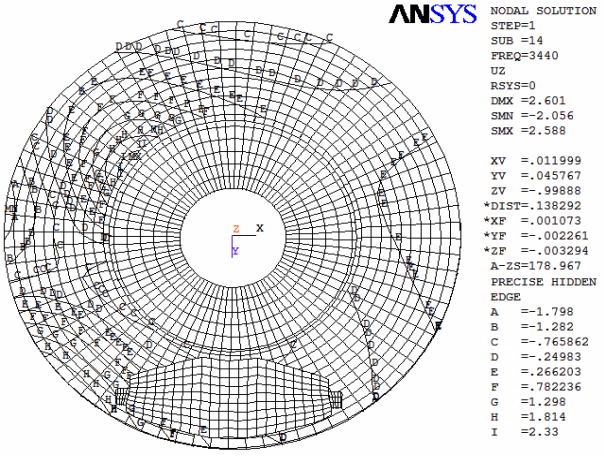

(e) Frequency 3440 Hz

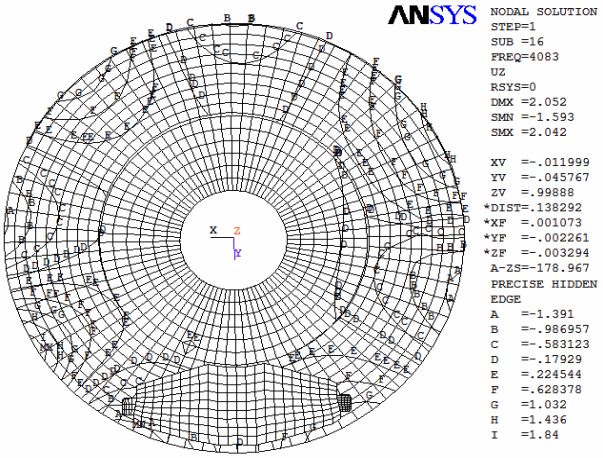

(f) Frequency 4083 Hz

Figure 11. Displacement contours at modes 1, 4, 6, 7, 14 and 16th respectively

In discussing the mode shape of the coupled ventilated disc brake system, it was found one or more of four cases as shown in Figure 12. In the first case, the upper ring of the ventilated rotor squealed only as shown in modes 1, 6, 7, 9, 12 and 16. The second case, the lower ring of the ventilated rotor squealed as clear in modes 4, 14, 18 and 27. The third case that the inboard pad (pad under the master piston) that lied on the upper ring of the rotor squealed between bending and twisting modes as obvious in modes 3, 5, 6, 7, 9, 10, 11, 12, 15, 16, 17, 21, 25 and 26. The fourth case that the outboard pad (pad under the

master fist) that lied on the lower ring of the rotor squealed also between bending and twisting modes as clear in modes 2, 8, 13, 19, 20, 22, 23 and 24. Generally, these Figures10 and 11 show the layout of the squealing frequency of each component in the coupled disc brake system. It was realized generally, the vibration modes were characterized by relative motions between the disc and the pad. Increasing the damping of the friction material may often solve the noise problem. However, if the characteristic vibration mode was a flexural mode, so-called secondary damping measure [48], the coated shims on the backplate could effectively solve the problem.

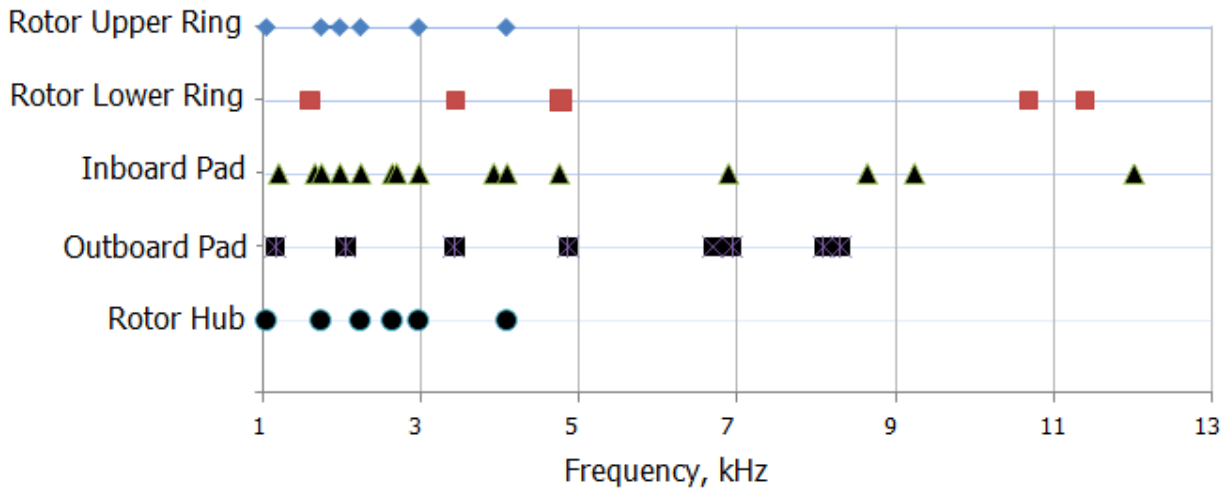

Figure 12. Eigen-frequencies of the coupled disc brake system components

In terms of squeal tendency, it was realized that the tendency of instability (TOI increased with increasing or decreasing the contact stiffness between the ventilated rotor and the two pads.

$$TOI = \sum_i \left(\frac{\text{Imaginary Part } (s_i)}{\text{Real Part } (s_i)} \times 1000 \right), \text{ Real part (si} > 0$$

This correlation was used by Dihua [5] to show the effect of different parameters on the tendency of the squeal. The physical meaning of the term (Imaginary (si)/Real (si)) is the damping ratio. That a mode had eigenvalue whose imaginary part was above zero meant the system was unstable and the damping value of that mode was negative. The tendency of squeal was 65 at contact stiffness 800 MN/m, 59 at contact stiffness 1000 MN/m, 64 at contact stiffness 1200 MN/m while was 69 at contact stiffness 1400 MN/m as shown in Figure 13. In studying the effect of contact stiffness on the stability of the system, it was found the stiffness to achieve the lowest instability was 1000 MN/m, which also could help in a further contact study. Figures 14 and 15 show the imaginary part (instability) against real part (frequency) for all contact stiffnesses 800, 1000, 1200 and 1400 MN/m respectively. The maximum imaginary part (instability reached at contact stiffness 800 MN/m was 520 sec^{-1} and 480 sec^{-1} at contact stiffness of 1000 MN/m. However, it reached 650 sec^{-1} at contact stiffness 1200 MN/m and 540 sec^{-1} at contact stiffness of 1400 MN/m. The maximum instability reached in this study was 480 sec^{-1} as seen in Figure 14 that was recorded at frequency 4083Hz.

Generally, the normal vibration modes of the ventilated disc brake rotors consisted of nodal diameters (nodal lines and circumferential circles (nodal circles). Figures 6 and 7 showed the modes layout of the rotor with constrained inner periphery. It was noted that as a results of the rotor's symmetry, the nodal lines (nodal diameters) for these modes had no preferred position [51]. The mode, which had a single nodal line (diameter), might rotate about the axis of the rotor through an arbitrary angle Figures 6 and 7. However, the mode, which had two nodal lines, the nodal lines might rotate together through an arbitrary angle without preference. In the case, where there were no nodal diameters, circumferential circles (nodal circle were found and this called disc coning phenomena or umbrella mode. It was shown in previous studies that the squeal of the rotor could happen at any diametral nodes [46].

The normal modes of the pad consisted of two types of modes. The first type was the bending type Figure 8-a and the second was the twisting type Figure 8-b. In some cases, the two types could be achieved together and on the contrary, the two types could not be achieved either. The properties of the

pad was the reason for the bending and twisting types of modes such as the young's modulus of the backplate and friction material and also the pad length [48].

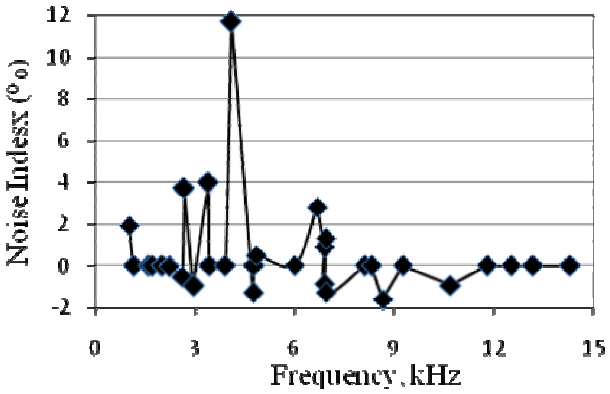

Figure 13. Contact Stiffness against Squeal Tendency

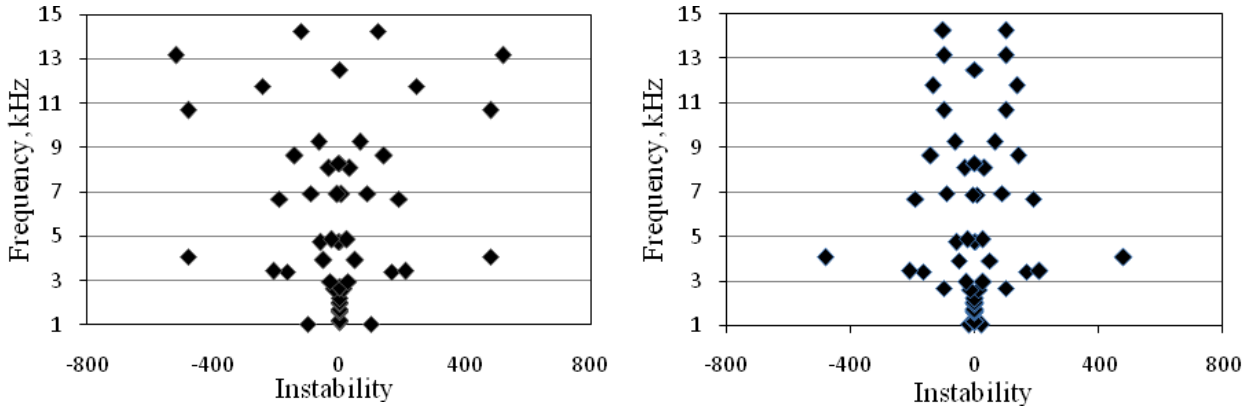

Figure 14. Real part against Imaginary part at contact stiffness 800 MN/m and 1000 MN/m

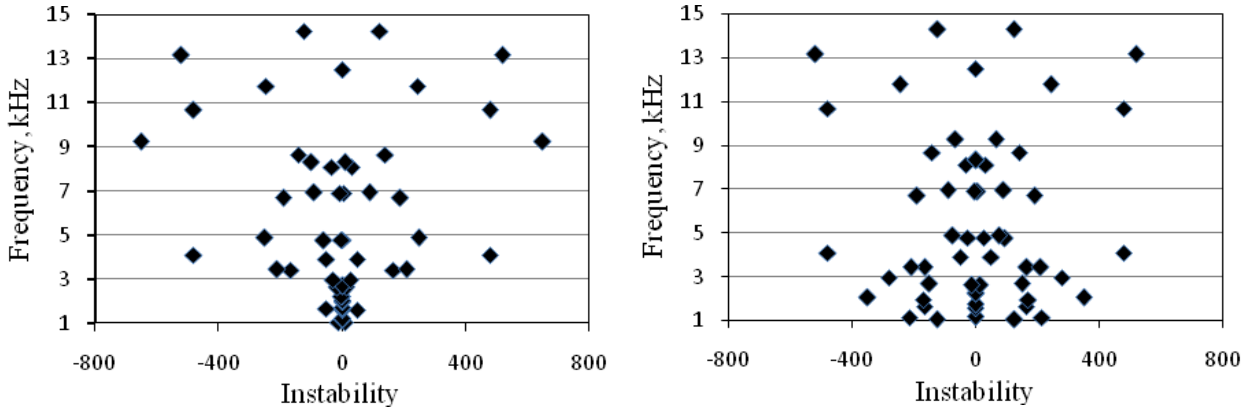

Figure 15. Real part against Imaginary part at contact stiffness of 1200 MN/m and 1400 MN/m

The individual finite element models of the pad and ventilated rotor were coupled for stability analysis to predict eigenvalue and eigenvector for the coupled system. The friction force between two rubbing surfaces was one of the most important key elements to understand and predict the system's instability [1, 49, 50]. It may induce negative damping or coupled component modes. It may also generate surface waves between the interfaces, which lead to stick-slip motion that causes dynamic instability. The friction force between two rubbing surfaces depended on the size of the contact area, contact stiffness, pressure, material properties and environmental influences [48]. It was shown from previous work that friction between two surfaces induced both in-plane and out-of-plane. The in-plane mode controlled the squeal frequency and the out-of-plane mode vibration generated noise. At the high squeal frequency

range, the squeal likely produced the energy exchanged between in-plane vibration and out-of-plane vibration of the rotor. Many high frequency squeals happened at the in-plane frequencies of rotors, particularly when the in-plane modes were coupled with out-of-plane modes of rotors [52].
The data plotted in Figures 14 and 15 have shown that modes with higher positive damping were most likely to produce audible brake squeal. An automotive brake system may possess many unstable vibration modes in the squeal frequency range 1-15 kHz. To compare the squeal propensity among unstable vibrational modes, the magnitude of the instability has been employed as a noise index [53-55]. So that, using the magnitude of the instability as a noise index implied high frequency squeal was more likely to occur than low frequency squeal. In this study, the noise index was defined as Yuan's definition [5] for each vibration mode;

$$\text{Noise Index (NI)} = \frac{\omega_j}{\sqrt{\omega_j^2 + \sigma_j^2}} \times 100\% .$$

The greater the (NI) the more likely the corresponding mode was considered to cause audible squeal noise. It is realized in Figure 16 that the maximum noise index is 11.7% at frequency 4083 Hz. However, the second high value of noise index is 4.3 % is at frequency 3440 Hz. The highest noise indexes were found at the maximum instabilities to confirm that the audible squeal noise could occur at the maximum instabilities as indicated by Yuan [5].

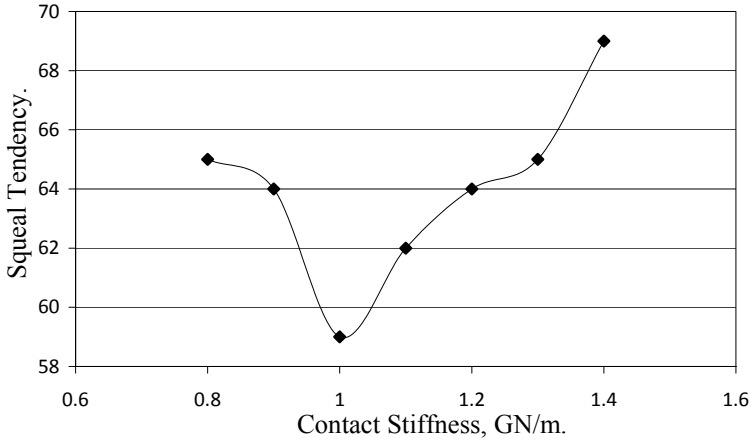

Figure 16. Noise Index against Frequency

9. Conclusion

The main conclusions from the work carried out summarized in the following points:

- The individual finite element model for the ventilated rotor showed 7 (seven) diametral modes for the eigenvalue analysis including 100 modes in the frequency range 1-15 kHz. It was recorded also one disc-coning phenomenon at the first mode. Furthermore, the individual finite element model of the pad showed 69 modes containing bending and twisting types of modes also in the frequency range 1-15 kHz and also a combination of the bending and twisting modes.
- The FEM of the coupled ventilated rotor and pad showed a good interaction between the non-linear contact and the linear modal analysis. It showed that the squeal occurred may be due to the geometrical coupling of the rotor and pad over the frictional interface where the circumferential friction forces were induced.
- The unsymmetric solver showed that the modes of the coupled disc-pad contained two types of mode. The first type was normal mode, which did not contain an imaginary part while the second type was complex mode that contained real and imaginary parts.
- The maximum squeal index was 11.7 % that occurred at mode 16 and frequency of 4083 Hz with instability of 480 sec^{-1}. The tendency of instability (TOI) for the system at contact stiffness of 1 GN/m was 59 that gave the lowest instability compared to the other contact stiffnesses used and also did not give ill-convergence.

References

[1] Matsushima, T. Masumo, H., Ito, S. and Nishiwaki, M. "FE analysis of low-frequency disk brake squeal (in case of floating type caliper)" SAE, Paper No. 982251, 1998.
[2] Nack, W.V. "Brake squeal analysis by finite elements" International Journal of Vehicle Design 23 (3-4), pp. 263–275, 2000.
[3] Matsui H, Murakami H, Nakanishi H, Tsunda Y. "Analysis of disc brake squeal" SAE 1992. paper 920553.
[4] Murakami H, Tsunada N , Kitamura T. "A study concerned with a mechanism of disc-brake squeal" SAE 1984. paper 841233.
[5] Dihua G. and Dongying J . "A study on disk brake squeal using finite element methods" SAE 1998, paper 980597.
[6] Baba H, Okade M and Takeuchi T. "Study on reducing low frequency brake squeal from modal analysis of mounting bracket" SAE Trans J Passenger Cars 1995; 104(6):2852–6.
[7] Bae JC and Wickert JA. "Free vibration of coupled disk-hat structures. Journal of sound and vibrations, 2000;235(1):117–32.
[8] Chen F, Chern J and Swayze J. "Modal coupling and its effect on brake squeal" SAE 2002, paper 2002-01-0922.
[9] Yi Dai and Teik C Lim "Suppression of Brake squeal noise applying finite element brake and pad model enhanced by spectral-based assurance criteria" Journal of applied acoustics 69 (2008), 196-214.
[10] Chen F, Tan CA and Quaglia RL. "Disc brake squeal – mechanism, analysis, evaluation and reduction/prevention" . SAE International ; 2005.
[11] Liles GD. "Analysis of disc brake squeal using finite element methods" SAE 1989. paper 891150.
[12] Shi TS, Dessouki O, Warzecha T, Chang WK and Jayasundera A. "Advances in complex eigenvalue analysis for brake noise" SAE 2001. paper 2001-01-1603.
[13] Kung SW, Saligrama VC and Riehle MA. "Modal participation analysis for identifying brake squeal mechanism" SAE 2000. paper 2000-01-2764.
[14] Blaschke P , Tan M and Wang A. "On the analysis of brake squeal propensity using finite element method" SAE 2000. paper 2000-01-2765.
[15] Lee YS, Brooks PC, Barton DC and Crolla DA. "A study of disc brake squeal propensity using a parametric finite element model". Proceedings of European conference on vehicle noise and vibration, IMechE, C521/009/98, 1998.
[16] Papinniemi A, Lai JCS, Zhao J and Loader L. "Brake squeal: a literature review" Journal of Applied Acoustics 2002;63:391–400.
[17] Kinkaid NM, O'Reilly OM and Papadopoulos P. "Automotive disc brake squeal" Journal of Sound and Vibration 2003;267:105–66.
[18] Watany M, Seoud SA, Saad A and Gawad IA. "Brake squeal generation" SAE Trans J Passenger Cars 1999;108(6):2730–9.
[19] Flint J. "The effect of distributed parameters examined in a model for simulation of disc brake squeal" SAE 2000, paper 2000-01-2766.
[20] Kido I, Kurahachi T. and Asai M. "A study on low-frequency brake squeal noise" SAE Trans J Passenger Cars 1996;105 (6):1382–7.
[21] Elbutch AM, Ibrahim IM. "Modeling and analysis of geometrically induced vibration in disc brakes considering contact parameters" SAE 1999, paper 1999-01-0143.
[22] Tanaka, S. Kazuhiko, K.Takeshi, I.Hidenobu, H "The compatibility of air disc brakes and S-cam brakes installed on combination vehicles" SAE, Paper No. 902201, pp 653-660, 1990.
[23] Samie, F. and Sheridan, D. C. "Contact Analysis for a passenger cars disc brakes" SAE Technical Paper No. 900005, 1990.
[24] Ibrahim Ahmed, Essam Allam, Mohamed Khalil and Shawkil Abouel-seoud "Automotive Drum Brake Squeal Analysis Using Complex Eigenvalue Methods" International Journal of Modern Engineering research (IJMER), Vol. 2, Issue 1, pp 179-199, Jan-Feb 2012.
[25] Ibrahim Ahmed, Sameh Metwally, Eid Mohamed and Shawki Aouel-Seoud "Influence of Surface Modification on Vehicle Disc Brake Squeal" SAE 2009-01-1977, SAE 2009 International Powertrains Fuels and Lubricants Meeting, June 15-17, 2009, Florence, Italy.

[26] Ibrahim Ahmed "Contact Behaviour of Vehicle Drum Brake by Using Finite Element Analysis" SAE 2007-01-2264, SAE 2007 Noise and Vibration Conference and Exhibitions, May 15-18, 2007, USA.
[27] Ibrahim Ahmed and S. Abouel Seoud "On the Analysis of Drum Brake Squeal Using Finite Element Method Technique" SAE 2006-01-3467, SAE 2006 Commercial Vehicle Engineering Congress & Exhibition, October 2006, USA.
[28] Ibrahim Ahmed "Studying the Contact Analysis Behaviour of Vehicle Drum Brake Using Finite Element Methods" SAE 2006-01-3561, Commercial Vehicle Engineering Congress and Exhibition, Chicago, Illinois, October 31-November 2, 2006, USA.
[29] Ibrahim Ahmed and S. Abouel Seoud "Drum Brake Squeal Analysis By Finite Element Method" SAE 2006-01-3211, 24th Annual Brake Colloquium and Exhibition, SAE , 2006 USA.
[30] Ibrahim L Ahmed "State Observers Design for Controlling the Vehicle Brake Dynamic Behaviour" 23rd Annual Brake Colloquium and Exhibition, SAE 2005-01-3946, Orlando, Florida October 9-12, 2005 USA.
[31] Ibrahim L Ahmed and Ahmed E Hassaneen "Degree of instability of Disc-Brake Parameters and its Effect on Brake Squeal; an Analytical Approach" Scientific Bulletin of Faculty of Engineering, Ain Shams University, Vol. 39, No. 2, June 30, 2004, Egypt.
[32] Abu Bakar, A. R. Ouyang, H. and Titeica, D. "Modeling and simulation of disc brake contact analysis and squeal" Submitted to Seminar on Advances Malaysian Noise, Vibration and Comfort, 2005.
[33] Rhee, S. K. Jacko, M. G. and Tsang, P. H. S. "The role of friction film in friction, wear and noise of automotive brakes" Wear, 246, pp. 89-97, 1991.
[34] Duffour, P. and Woodhouse, J. " Instability of systems with a frictional point contact. Part 2: model extensions" Journal of Sound and Vibration 271, pp. 391–410, 2004.
[35] Sherif, H.A. "Investigation on effect of surface topography of pad/disc assembly on squeal generation" Wear 257, pp. 687–695, 2004.
[36] Massi, F. Berthier, Y. and Baillet, L. "Contact surface topography and system dynamics of brake squeal " Wear, 2008.
[37] Loading "Ansys User's Manual Revision 12 " Swanson Analysis System, Inc. P.O. Box 65, Johnson Road, Houston, USA.
[38] Contact Analysis "Ansys User's Manual Revision 12 " Swanson Analysis System, Inc. P.O. Box 65, Johnson Road, Houston, USA.
[39] Modal Analysis "Ansys User's Manual Revision 12 " Swanson Analysis System, Inc. P.O. Box 65, Johnson Road, Houston, USA.
[40] Elements Library "Ansys User's Manual Revision 12 " Swanson Analysis System, Inc. P.O. Box 65, Johnson Road, Houston, USA.
[41] "Ansys User's Manual Revision 12 " Swanson Analysis System, Inc. P.O. Box 65, Johnson Road, Houston, USA.
[42] Modelling and Meshing Guide "Ansys User's Manual Revision 12 " Swanson Analysis System, Inc. P.O. Box 65, Johnson Road, Houston, USA.
[43] Unsymmetric Solver "Ansys User's Manual Revision 12 " Swanson Analysis System, Inc. P.O. Box 65, Johnson Road, Houston, USA.
[44] Theory Manual "Ansys User's Manual Revision 12 " Swanson Analysis System, Inc. P.O. Box 65, Johnson Road, Houston, USA.
[45] John D. Fieldhouse, and Peter Newcomb "An Investigation Into Disc Brake Squeal Using Holographic Interferometry" 3rd International EAEC Paper No.91084, Strasborg, June 1991.
[46] Ripin, Z.B.M. "Analysis of Disc Brake Squeal Using the Finite Element Methods" Ph.D. thesis, Leeds, UK, 1995.
[47] Guyan, R.J. "Reduction of Stiffness and Mass Natrices" AIAA Journal, Vol. 3, No. 2, pp.380, Feb. 1995.
[48] Klaus Schiffner, and Andreas Rinsdorf "Practical Evaluation and FEM-Modeling of a Disc Brake" SAE, No. 933071, pp 2450-2460, 1993.
[49] Day A.J. and Kim S.Y. "Noise and Vibration Analysis of S-cam Drum Brake" Proc. ImechE, Vol 210, pp. 35-43, 1996.
[50] Alex C. Lee "Study of Disc Brake Noise Using Multi-body Mechanism with Friction Interface." ASME, DE-Vol 49, Friction-Induced Vibration, Chatter, Squeal and Chaos, pp 99-105, 1992.

[51] Mottershead J.E. and Chan S.N. “Brake Squeal-An Analysis of Symmetry and Flutter Instability” ASME, Design Engineering Vol. 49, Friction Induced Vibration, Chatter, Squeal and Chaos, AME 1992.
[52] John D. Fieldhouse, and Peter Newcomb “The Application of Holographic Interferometry to the Study of Disc Brake Noise” SAE, No. 930805, pp1256-1270, 1993.
[53] Hideto Murakami, Naomasa Tsunada and Terukiyo Kitamura “A Study Concerned with a Mechanism of Disc Brake squeal” SAE No. 841233, pp. 5.604-5.616, 1984.
[54] North M.R. “Disc Brake Squeal” IMechE, C38/76, pp.169-176, 1976.
[55] Millner, N. “An Analysis of Disc Brake Squeal.” SAE, No. 780332, 1978.

Ahmed Abdel-Naser is a technical consultant at the Ministry of Justice, Egypt. He obtained his B.Sc. of Automotive and Tractors Engineering from Minia Unversity in Minia, Egypt on 2003. He is doing a research at the Faculty of Engineering, Helwan University, Cairo-Egypt. His Master is titled Modal and Contact Analysis of Ventilated Brake. Mr. Ahmed is a member of Egyptian Engineering Syndicates, Egyptian Society of Automotive Engineers.
E-mail address: abd_elnaser666@yahoo.com

Ibrahim Ahmed is an Associate Professor of Vehicle Dynamic and Control at the Faculty of Industrial Education, Helwan University in Egypt. He is currently the Head of Automotive and Tractors Technology Department. He obtained his B.Sc. and M.Sc. of Automotive Engineering from Helwan Unversity in Cairo, Egypt on 1990 and 1995 respectively followed by another M.Sc. from Eindhoven University 1997. He obtained also the PhD from University of Northumbria at Newcastle Upon Tyne , UK in 2002. He has about 35 papers in the field of Vehicle Dynamics and Tribology. He has many contributions in the field of Noise, Vibration and Harshness (NVH). Dr Ahmed is a member of Egyptian Engineering Syndicates, Egyptian Society of Automotive Engineers and a full member in the American Society of Automotive Engineers SAE.
E-mail address: ilmahmed1968@yahoo.co.uk

Essam M. Allam is an Associate Professor of Vehicle Dynamic and control at Helwan University. He obtained the B.Sc., M.Sc. & PhD degrees in Automotive Engineering from Helwan University in 1995, 2001 & 2005 respectively. He has about 20 publications in the field of Vehicle Dynamic and control. In addition his current research projects are focused on development of the vehicle noise and vibration from point of view of control and maintenance. Dr. Allam is a member of the Egyptian Society of Engineers.
E-mail address: emmorsyf@yahoo.com

Sabry Allam is an Associate Professor of Vehicle Dynamic and Control at the Faculty of Industrial Education, Helwan University in Egypt. He is currently a researcher at the Aeronautical and Vehicle Engineering Department, The Royal Institute of Technology, Stockholm, Sweden. He obtained his B.Sc. and M.Sc. of Automotive Engineering from Helwan University in Cairo, Egypt on 1989 and 1994 respectively. He obtained also the PhD from The Royal Institute of Technology, Stockholm, Sweden in 2005. He has many papers in the field of Vehicle Dynamics and also has many contributions in the field of Noise, Vibration and Harshness (NVH). Dr Allam is a member of Egyptian Engineering Syndicates, Egyptian Society of Automotive Engineers.
E-mail address: mail@mail.com

Shawki A. Abouel-seoud is a Professor of Vehicle Design and Dynamics at Helwan University. He obtained the B.Sc. from Helwan University in 1969 and the Ph.D. degree in Mechanical Engineering from Birmingham University, U.K. in 1979. He has about 80 publications in the field of Vehicle Design and Dynamics. In addition, his current research projects are focused on development of the vehicle noise and vibration from point of view of control and maintenance. Prof. Abouel-seoud is Member of the Egyptian Society of Engineers and Member of the scientific committee for the promotion of University Staff (associate professors).
E-mail address: s_a_seoud@hotmail.com

